Mon. Not. R. Astron. Soc. **000**, 1–19 (2012) Printed 23 January 2013 (MN LATEX style file v2.2)

The sub-stellar birth rate from UKIDSS

A. C. Day-Jones[1,2⋆], F. Marocco[2], D. J. Pinfield[2], Z.H. Zhang[2], B. Burningham[2], N. Deacon[4], M.T. Ruiz[1], J. Gallardo[5], H.R.A. Jones[2], P.W.L. Lucas[2],J.S. Jenkins[1], J. Gomes[2], S.L. Folkes[3,2], J.R.A. Clarke[3,2].

[1] *Departamento de Astronomia, Universidad de Chile, Camino del Observatorio 1515, Santiago, Chile.*
[2] *Centre for Astrophysics Research, University of Hertfordshire, College Lane, Hatfield, Hertfordshire, UK.*
[3] *Departamento de Fisica y Astronomia, Facultad de Ciencias, Universidad de Valparaiso, Av.Gran Bretana 1111, Valparaiso, Chile.*
[4] *Max Planck Institute for Astronomy, Knigstuhl, 17. D-69117, Heidelberg, Germany.*
[5] *ALMA, Alonso de Cordova 3107, Vitacura, Santiago, Chile.*

ABSTRACT

We present a new sample of mid L to mid T dwarfs with effective temperatures of 1100 to 1700 K selected from the UKIDSS Large Area Survey and confirmed with infrared spectra from X-Shooter/VLT. This effective temperature range is especially sensitive to the formation history of Galactic brown dwarfs and allows us to constrain the form of the sub-stellar birth rate, with sensitivity to differentiate between a flat (stellar like) birth rate, and an exponentially declining form. We present the discovery of 63 new L and T dwarfs from the UKIDSS LAS DR7, including the identification of 12 likely unresolved binaries, which form the first complete sub-set from our program, covering 495 sq degrees of sky, complete to J=18.1. We compare our results for this sub-sample with simulations of differing birth rates for objects of mass 0.10-0.03$M_{\odot}$ and ages 1-10Gyrs. We find that the more extreme birth rates (e.g. a halo type form) can likely be excluded as the true form of the birth rate. In addition we find that although there is substantial scatter we find a preference for a mass function, with a power-law index, α in the range $-1 < \alpha < 0$ that is consistent (within the errors) with the studies of late T dwarfs.

Key words: low mass stars, brown dwarfs.

1 INTRODUCTION

The distribution of star formation with mass and time are key pieces of observational evidence for understanding star formation in the galaxy. The former is described by the initial mass function (IMF; Salpeter 1995), which can be described as a power-law of the form $\psi(M) \propto M^{-\alpha}$, with $\alpha = 2.35$, and has been determined across the stellar mass regime by measuring the luminosity function for a population of stars, and applying a mass-luminosity relation, which should account for metallicity variations. Since brown dwarfs never reach the main sequence, this determination is complicated in the sub-stellar regime by the lack of a unique mass-luminosity relationship. Instead the $T_{\rm eff}$ and luminosity are dependent on mass *and* age (Allard et al. 1997). This means that the luminosity function and $T_{\rm eff}$ distributions of field brown dwarfs depend not only on the mass function, but also on their formation history (Chabrier 2002). Indeed, extending the Salpeter mass function to sub-stellar objects one would expect many more brown dwarfs than stars, which is not seen by observations of late M and L dwarfs (e.g. Reid, Gizis & Hawley 2002). In addition it is not totally apparent that the full field population of brown dwarfs is populated by objects that formed through a cloud fragmentation process. There are a number of ways that brown dwarfs could form that are different to the canonical ways in which stars are thought to form. There are at least four different formation mechanisms that have been suggested, such as formation through the "ejection" of pre-stellar cores (Reipurth & Clarke 2001; Bate, Bonnell & Bromm 2002; Delgado-Donate, Clarke & Bate 2003; Sterzik et al. 2003) or through "turbulence", or turbulent fragmentation (Padoan & Nordlund 2002; Padoan & Nordlund 2004). Other theories include that of "disc fragmentation", forming sub-stellar cores from an initially massive

⋆ E-mail:adjones@das.uchile.cl. Based on observations made with ESO telescopes at the La Silla Paranal Observatory under programmes 086.C-0450, 087.C-0639 & 088.C-0048.

pre-stellar core via fragmentation of a large circumstellar disk (Boffin et al. 1998; Bate, Bonnell & Bromm 2003; Whitworth & Goodwin 2005; Whitworth & Stamatellos 2006) and "photo-erosion", where sub-stellar objects form in the presence of a higher mass star embedded in a HII region (Whitworth & Zinnecker 2004). As the formation mechanisms could indeed be different for sub-stellar objects it is thus important to define the mass function and formation history in the sub-stellar regime if we wish to fully understand their contribution to the Galactic population.

Young clusters have been the target of many studies seeking to measure the sub-stellar IMF since their known ages and metallicities allow the use of a mass-luminosity relation based on a single coeval age (e.g. Caballero et al. 2009; Oliveira, Jeffries & van Loon 2009; Luhman et al. 2007; Lodieu et al. 2007a). Although these clusters allow a relatively direct measurement of the sub-stellar IMF, they also introduce their own problems, since the initial conditions and accretion histories of individual objects introduce uncertainties regarding the ages, and hence masses, of such young objects (e.g. Baraffe 2010). As it is difficult to determine the age of field brown dwarfs, unless they have fiducial constraints on their age as binaries (e.g. Burningham et al. 2009; Zhang et al. 2010; Burningham et al. 2010a; Day-Jones et al. 2011; Murray et al. 2011) or as members of moving groups (Gálvez-Ortiz et al. 2010; Clarke et al. 2010), estimating the mass function of field brown dwarfs requires a knowledge of their formation history. This is often assumed to be the same as that for stars (constant with time; Miller & Scalo 1979), but is unconstrained in the sub-stellar regime. The first attempt to measure the sub-stellar mass function was made by Reid et al. (1999) from preliminary results from 2MASS data based on only 17 L dwarfs. More recently, with the discovery of late T dwarfs several other groups have made measurements of the sub-stellar mass function in the disc. These have all generally been with small sample sizes or cover only L dwarfs (e.g. Cruz et al. 2007) or only T dwarfs (e.g. Burningham et al. 2010b; Kirkpatrick et al. 2012; Metchev et al. 2008). Those that have considered the full temperature regime across the L and T dwarf spectral types (e.g Reylé et al. 2010) suffer from large associated errors and large bin sizes in order to get large enough sampling.

In order to characterise the form of the sub-stellar formation history a large sample of brown dwarfs is required. With modern large-scale near and mid infrared surveys, such as the 2MASS (Skrutskie et al. 2006), UKIDSS (Lawrence et al. 2007), VISTA (Emerson & Sutherland 2003) and WISE (Wright et al. 2010), which have identified large numbers of brown dwarfs (Kirkpatrick et al. 2000; Hawley et al. 2002; Pinfield et al. 2008; Burningham et al. 2010b; Kirkpatrick et al. 2011, Cushing et al. 2011) it is now possible to provide the necessary sample of such objects. This paper outlines our efforts to use the UKIDSS Large Area Survey to empirically constrain the Galactic brown dwarf formation history. We discuss past and present simulations of the formation history in §2. In §3 the selection of our sample of L and T dwarfs from the UKIDSS LAS, §4 gives details of the observations and data reduction. In §5 we present the spectroscopy and spectral types of our sample and investigate potential unresolved binarity. In §6 we compare our first observations with simulations and look at constraints that can be placed on the formation history of Galactic brown dwarfs. Finally we summarize our findings in § 7.

2 SIMULATIONS OF THE FORMATION HISTORY

Simulations of the effect of how the birth rate affects the luminosity function have been performed by several authors. Based on model data and direct comparisons with DENIS and 2MASS observations, Chabrier (2002) made simulations using two different initial mass functions and birth rates. Namely a flat, or constant birth rate, which is the simplest form and supported by the work of Miller & Scalo (1979), who suggest that the birth rate does not depend strongly on the gas density, and is approximately consistent across the Galactic disc. They also consider an exponential form where the formation decreases with time. These are considered with initial mass functions of a power-law form derived by Chabrier (2001), and a log normal and exponential form which essentially give the same result when considering the effects from the birth rate. Burgasser (2004) considered a wider range of birth rates in his monte-carlo simulations considering, in addition to a flat and exponential forms, an "empirical" birth rate, which is the same as that measured for stars by Rocha-Pinto et al. (2000), which represents ′bursts′ of formation at peak internavls of 0-1, 2-5 and 7-9Gyrs. This formation history scenario is also supported by the more recent work of the stellar formation history by Cignoni et al. (2006) and Wyse (2008). In addition Burgasser (2004) also considers a "cluster" birth rate which assumes a flat, but stochastic (i.e in a number of clusters) formation, which produces a similar result to a flat formation scenario. Finally he considers a "halo" type birth rate, that includes formation within a 1 Gyr burst, 9 Gyr in the past, in an attempt to explain a number of subdwarf brown dwarfs that have been identified (e.g. Burgasser et al. 2003; Lodieu et al. 2010). This scenario gives a radically different $T_{\rm eff}$ distribution for L and T dwarfs compared to the other scenarios, and seems unlikely since we are now seeing a larger number of L dwarfs identified in very young clusters (e.g. Taurus; **?**, Quanz et al. 2010, Cameleon; Luhman 2007, Serpens; Lodieu et al. 2002, TWA Hydra; Chauvin et al. 2004, Upper Sco; Lodieu et al. 2008, Lafreniére et al. 2008) .

More recent simulations performed by Deacon & Hambly (2006) looked more specifically at L and T dwarfs from the UKIDSS LAS. They produced simulations that take into account several IMFs including a flat, log normal and different power laws (α =+1.0, 0, and -1.0), combined with different exponential forms of the birth rate, similarly to those described above. These simulations also included the effect of Galactic disc heating, which had not been included in previous simulations of the birth rate. A histogram of these simulations (a log normal form of the IMF with different birth rates) is shown in Fig. 1. These simulations are similar to those of Allen et al. (1995) (see their fig.2). with the main differences arising from the differences in the normalisation of the space density. Allen et al. (1995) uses 0.35 stars pc^{-3} M$_{\odot}$ according to Reid & Gizis (1997), where as the simulations based on those of Deacon & Hambly (2006) use 0.0024 stars

$pc^{-3}M_{\odot}$ according to Deacon, Nelemans & Hambly (2008). In addition changes also arise from the different values used for their birth rates, and as such are similar and show the same trends but are not directly comparable.

It can be clearly seen in the Deacon & Hambly (2006) simulations that the sub 1000K region is extremely sensitive to the IMF, but relatively insensitive to the birth rate, while the 1100-1500K, corresponding to the mid-L to mid-T spectral range is most sensitive to differing birth rates. While several hundred brown dwarfs have been identified in large area surveys such as 2MASS and SDSS, they were more sensitive to the detection of L dwarfs and produced only a few tens of early T dwarfs. As such they could not provide the population needed to study and constrain the birth rate. The UKIDSS LAS probes to greater depth across the L and T dwarf spectral types and can provide a statistically robust sample spanning the mid-L to mid-T region, which is most sensitive to the effects of the form of the birth rate. We thus select a sample of mid L – mid T dwarfs from the UKIDSS LAS in order to compare the space density with that of late T's (Burningham et al. 2010a) and late Ms and earlier Ls to measure the birth rate.

3 SAMPLE SELECTION

We select our sample from DR7 of the UKIDSS LAS survey, selecting objects with declination $\leqslant 20$ degrees, $J < 18.1$ and $Y - J > 0.8$ following the criteria of Hewett et al. (2006), who demonstrate that using a $Y - J > 0.8$ colour criterion is largely free of M dwarfs while including all L dwarfs §6.1. We also used the following quality flags to ensure that selected objects are point sources and are not likely cross talk effects, or sit at the edge of the detector, such that the following quality flags were used:

$$\begin{gathered}(\text{priOrSec}= 0 \text{ OR priOrSec} = \text{frameSetID})\\ \text{yppErrBits} < 256\\ \text{j}_1\text{ppErrBits} < 256\\ \text{hppErrBits} < 256\\ -3.0 < \text{mergedClass} < -0.5\\ -3.0 < \text{mergedClassStat} < 3.0\\ \text{yEll} < 0.45\\ \text{j}_1\text{1Ell} < 0.45\end{gathered}$$

This list of candidates was then cross-matched against SDSS DR7 to identify objects with optical counterparts. Using a matching radius of 4 arcsec we selected objects with optical counterparts according to the criteria below, based on those of Schmidt et al. (2010), who provide colours from an unbiased spectroscopically complete sample. Since our NIR colour selection effectively removes all contaminant field M dwarfs this allowed us to be more liberal with our redder sources ($J - K > 1.0$) in terms of our $z - J$ colour selection, and allows for larger uncertainties in the i' band as we are probing the faint end of SDSS. We also required Y and J photometry to have errors not greater than 3σ and detections in $H \geqslant 14.5$, such that this search space would not have been probed by 2MASS. In addition we also consider K band non-detections, if their $z - J$ colour passes our following criteria:

$$\begin{gathered}J \leqslant 18.1\\ Y - J \geqslant 0.8\\ z - J \geqslant 2.4 \text{ and } (J - K \geqslant 1.0 \text{ or no } K \text{ detection}) \text{ OR}\\ z - J \geqslant 2.9 \text{ and } (J - K < 1.0 \text{ or no } K \text{ detection})\end{gathered}$$

We then removed objects with the following:

$$\begin{gathered}i - z < 2.0 \text{ and } \sigma(i - z) < 0.35\\ i - J < 4.7 \text{ and } \sigma(i - j) < 0.2\\ z - K < 3.5 \text{ and } J - K > 1.0 \text{ and } \sigma(z - K) < 0.2\end{gathered}$$

As mid-T dwarfs typically have $z' - J > 3.0$ (e.g.Pinfield et al. 2008) some objects will be too faint for detection in SDSS, we thus include these SDSS non-detections. All objects were then visually inspected to remove any possible miss matches or cross-talk. We also cross matched our sample with known L and T dwarfs in dwarfarchives and retain those that have spectral types of $\geqslant$L4 (to be consistent with our completeness, see §6.1), giving a total sample size of 324 from 2000deg^2 of UKIDSS LAS (DR7) sky. In this work we consider a sub-sample from a smaller are of 495 sq degrees of sky in the RA and DEC range, RA=22 to 4 hr and DEC=-2 to 16 deg. This includes 76 L and T dwarfs, 13 of which were previously identified (and spectrally typed as L4-T4), 5 of these have been re-observed and 63 new L and T dwarfs. We show photometric information of this sub-sample in Fig. 2 and Table. 1, which are discussed and analysed further in the following sections.

4 OBSERVATIONS & DATA REDUCTION

Spectroscopic observations of candidates from our sub-sample, were obtained with X-shooter on the Very Large Telescope during Nov 27-31 2010, Feb 22-26, June 5-9 2011 and Sep 18-22 2011, under the ESO programs 086.C-0450(A/B) and 087.C-0639(A/B). We used the echelle slit mode, which covers the wavelength range 300-2500nm. This is split into three separate arms, the UVB (300-550nm), VIS (550-1000nm) and NIR (1000-2500nm). Using slit widths of 1.0 arcsec for the UVB arm and 0.9 arcsec for the VIS and NIR arms, we took four individual integrations in an ABBA pattern (See Table. 2 for integration times). We note that we do not detect any significant flux in the UVB wavelength range for members of our sample and as such we do not show the details for this arm. We took telluric standard stars after every second target, which were paired together so they were in roughly the same airmass. Sky flats and arc frames were also taken at the beginning of every night.

The data were reduced using the ESO X-shooter pipeline (version 1.3.7). The pipeline removes non-linear pixels, subtracts the bias (in the VIS arm) or dark frames (in the NIR arm) and divides the raw frames by flat fields. Images are pair-wise subtracted to remove sky background. The pipeline then extracts and merges the different orders in each arm, rectifying them using a multi-pinhole arc lamp (taken during the day-time calibration) and correcting for the flexure of the instrument using single-pinhole arc lamps (taken at night, one for each object observed). Telluric stars are reduced in the same way, except that sky subtraction is done by fitting the background (as tellurics are not observed in nodding mode). The spectra were telluric corrected and flux calibrated using IDL routines, following a standard procedure: first the telluric spectrum is cleared of HI absorption lines (by interpolating over them) and scaled to match the measured magnitudes; then is divided by a blackbody curve for the appropriate temperature, to obtain the

Table 1. Photometry of sub-sample.

Name	ID	RA	DEC	J[1]	Y-J[1]	J-H[1]	J-K[1]	z-J[1,2]	i-z[2]
ULAS J0006+1540	BRLT1	00:06:13	+15:40:21	17.88	1.08	1.16	1.73	2.73	3.55
ULAS J0010+0100	BRLT2	00:10:41	+01:00:13	18.09	1.27	0.63	1.38	2.71	1.42
ULAS J0018-0025	BRLT3	00:18:37	-00:25:59	17.67	1.06	1.06	-	2.61	2.83
ULAS J0024+1347	BRLT6	00:24:06	+13:47:05	18.02	1.26	0.69	1.50	6.04	0.62
ULAS J0027+1423	BRLT7	00:27:07	+14:23:49	17.98	0.98	0.61	1.12	2.43	2.23
ULAS J0028+1423	BRLT8	00:28:28	+14:23:49	17.56	1.38	0.95	1.72	2.72	2.50
ULAS J0029+1456	BRLT9	00:29:12	+14:56:05	17.56	1.25	0.64	1.23	2.41	2.14
SDSSp J0033+1410[a]	BRLT10	00:33:00	+14:10:37	16.65	1.18	0.96	1.64	2.78	3.66
ULAS J0037-0054	BRLT12	00:37:16	-00:54:05	18.09	1.36	0.76	1.42	2.71	1.79
ULAS J0043+1411	BRLT14	00:43:56	+14:11:18	17.33	1.09	0.64	1.21	2.42	2.05
ULAS J0047+1546	BRLT15	00:47:57	+15:46:41	17.83	1.29	0.66	1.41	-	-
ULAS J0050-0003	BRLT16	00:50:38	-00:03:37	17.86	1.17	0.79	1.34	2.70	1.98
ULAS J0100+0620	BRLT18	01:00:36	+06:20:44	17.77	0.87	0.86	1.43	-	-
ULAS J0105+1429	BRLT20	01:05:32	+14:29:32	18.01	1.25	0.54	1.18	2.59	2.33
ULAS J0111-0105	BRLT21	01:11:52	-01:05:34	17.34	1.30	0.81	1.41	3.00	1.96
ULAS J0112+1536	BRLT22	01:12:50	+15:36:58	18.00	1.01	0.59	1.14	-	-
ULAS J0116+1443	BRLT24	01:16:45	+14:43:35	17.96	1.35	0.95	1.66	-	-
SDSS J0127+1354[b]	BRLT26	01:27:44	+13:54:21	16.77	1.19	0.86	1.59	2.85	2.57
ULAS J0128-0041	BRLT27	01:28:14	-00:41:54	17.59	0.87	0.69	1.10	2.89	3.65
ULAS J0132+0552	BRLT30	01:32:44	+05:52:32	16.41	1.35	0.93	1.66	2.89	2.03
ULAS J0136+0717	BRLT31	01:36:20	+07:17:38	18.01	1.45	0.91	1.53	-	-
ULAS J0138-0104	BRLT32	01:38:08	-01:04:17	18.01	1.31	0.67	-	2.81	1.59
ULAS J0141+1318	BRLT33	01:41:03	+13:18:33	17.95	1.51	0.85	1.37	2.59	1.87
ULAS J0148+1400	BRLT35	01:48:12	+14:00:28	17.97	1.12	0.81	1.42	3.52	-0.16
ULAS J0149+1441	BRLT37	01:49:27	+14:41:08	18.04	1.27	0.94	1.72	2.55	2.90
ULAS J0150+1359[c]	-	01:50:24	+13:59:24	17.73	1.08	-0.38	-0.12	-	-
SDSS J0151+1244[a]	BRLT38	01:51:42	+12:44:29	16.39	1.02	0.79	1.10	-	-
ULAS J0151+1346	BRLT39	01:51:44	+13:46:46	17.66	1.24	0.82	1.57	2.62	2.89
ULAS J0200+0658	BRLT42	02:00:03	+06:58:08	17.93	1.18	0.73	1.22	-	-
SDSS J0203-0108[d]	BRLT44	02:03:33	-01:08:12	17.69	1.30	0.81	1.42	2.77	3.56
ULAS J0203-0102[e]	-	02:03:36	-01:02:31	18.05	1.09	-0.29	-0.11	-	-
ULAS J0205+1421	BRLT45	02:05:30	+14:21:14	17.99	1.15	0.73	1.06	2.71	4.47
ULAS J0206+0549	BRLT46	02:06:04	+05:49:59	17.92	1.06	0.50	1.11	2.48	1.92
SDSS J0207+0000[a]	-	02:07:42	+00:00:56	16.73	1.29	-0.07	0.01	-	-
ULAS J0247-0107	BRLT48	02:47:03	-01:07:01	17.77	1.43	0.94	1.77	-	-
ULAS J0255+0616[h]	BRLT50	02:55:45	+06:16:56	17.99	1.16	-0.68	-	-	-
ULAS J0259+0549	BRLT51	02:59:41	+05:49:35	18.02	1.25	0.83	1.54	-	-
ULAS J0314+0453	BRLT52	03:14:52	+04:53:46	17.30	1.29	0.91	1.71	3.06	2.00
ULAS J0320+0617	BRLT56	03:20:00	+06:17:41	17.79	1.46	0.75	1.39	-	-
ULAS J0320+0618	BRLT57	03:20:42	+06:18:37	18.06	1.21	0.58	1.15	2.43	1.93
ULAS J0321+0545	BRLT58	03:21:43	+05:45:24	17.33	1.22	0.73	1.37	2.74	2.34
ULAS J0323+0613	BRLT60	03:23:54	+06:13:52	17.64	1.37	0.65	1.33	-	-
SDSS J0325+0425[f]	-	03:25:53	+04:25:40	16.02	1.10	-0.22	-0.43	-	-
ULAS J0330+0556	BRLT62	03:30:06	+05:56:53	17.95	1.56	1.10	2.00	-	-
ULAS J0330+0426	BRLT64	03:30:37	+04:26:58	17.29	1.33	0.85	1.54	2.69	2.16
ULAS J0341+0423	BRLT66	03:41:50	+04:23:25	16.85	1.44	0.90	1.65	2.93	2.12
ULAS J2157+0056	BRLT305	21:57:00	+00:56:15	17.85	1.41	0.98	1.75	2.77	1.66
ULAS J2159+0033	BRLT306	21:59:20	+00:33:10	17.73	1.36	0.74	1.37	2.76	2.51
ULAS J2209-0053	BRLT307	22:09:17	-00:53:00	18.01	1.34	0.74	1.37	2.48	2.31
ULAS J2229+0102	BRLT311	22:29:58	+01:02:17	17.88	1.22	0.39	0.67	-	-
ULAS J2233+0022	BRLT312	22:33:48	+00:22:14	18.07	1.05	0.71	1.43	3.45	0.42
ULAS J2236+0111	BRLT313	22:36:37	+01:11:32	17.11	1.34	0.87	1.64	3.04	2.03
ULAS J2237+0716	BRLT314	22:37:57	+07:16:57	17.49	1.38	1.04	1.84	2.97	2.73
ULAS J2240+0008	BRLT315	22:40:52	+00:08:22	17.82	1.46	0.70	1.24	2.44	2.03
ULAS J2249+0715	BRLT316	22:49:23	+07:15:28	18.09	1.55	0.55	1.23	-	-
ULAS J2250+0808	BRLT317	22:50:16	+08:08:22	15.50	1.17	0.46	0.99	2.74	2.11
ULAS J2251-0007	BRLT318	22:51:15	-00:07:24	17.95	1.26	0.60	1.46	3.20	0.97
ULAS J2256+0724	BRLT320	22:56:31	+07:24:39	17.94	1.48	0.68	1.21	2.71	2.45
ULAS J2302+0700	BRLT321	23:02:03	+07:00:39	17.62	1.33	0.25	0.11	-	-
ULAS J2303+0058	BRLT322	23:03:59	+00:58:07	17.82	1.21	0.83	1.67	2.86	2.59
ULAS J2304+1301	BRLT323	23:04:25	+13:01:11	16.69	1.31	0.77	1.49	2.78	2.06
ULAS J2304+0804	BRLT325	23:04:34	+08:04:01	17.89	1.23	0.41	0.67	-	-

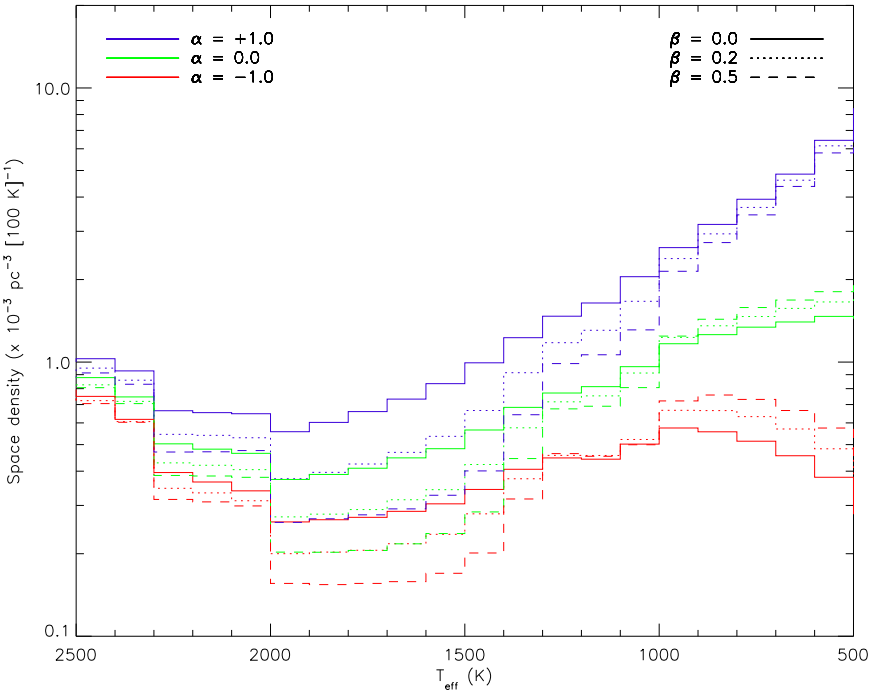

Figure 1. Monte-Carlo simulations of differing IMFs, where $\psi(M) \propto M^{-\alpha}$ for values of $\alpha = +1.0, 0.0$ and -1.0 and birth rates $\beta = 0.0, 0.2, 0.5$, based on the simulations from Deacon & Hambly (2006).

Table 1 continued. Photometry of sub-sample.

Name	ID	RA	DEC	J[1]	Y-J[1]	J-H[1]	J-K[1]	z-J[1,2]	i-z[2]
ULAS J2306+1302[c]	-	23:06:01	+13:02:25	17.57	1.39	-0.43	-0.46	-	-
ULAS J2312+0006	BRLT328	23:12:37	+00:06:02	17.65	1.30	0.60	1.25	2.62	2.07
ULAS J2316+0100	BRLT330	23:16:46	+01:00:13	17.95	1.15	0.69	1.25	3.13	1.94
ULAS J2320+1448[g]	-	23:20:35	+14:48:29	16.79	1.35	-0.35	-0.61	-	-
ULAS J2321-0045	BRLT331	23:21:23	-00:45:57	18.00	1.40	0.40	0.88	2.52	2.44
ULAS J2321+1354[g]	-	23:21:23	+13:54:54	16.72	1.20	-0.43	-0.44	-	-
ULAS J2323+0005	BRLT332	23:23:00	+00:05:42	18.01	1.15	0.74	1.15	2.53	2.17
ULAS J2323+0719	BRLT333	23:23:15	+07:19:31	17.30	1.20	0.75	1.10	3.05	3.38
ULAS J2327+1517	BRLT334	23:27:16	+15:17:30	16.20	1.34	0.85	1.52	2.97	2.13
ULAS J2327+0102	BRLT335	23:27:32	+01:02:53	18.07	1.19	0.83	1.46	-	-
ULAS J2328+1345[c]	-	23:28:02	+13:45:44	17.75	1.26	-0.42	-0.54	-	-
ULAS J2330+1403	BRLT338	23:30:02	+14:03:30	17.37	1.23	0.57	1.26	-	-
ULAS J2347-0110	BRLT343	23:47:17	-01:10:09	17.57	1.25	0.85	1.67	2.70	2.35
ULAS J2356+0754	BRLT344	23:56:18	+07:54:20	18.09	1.51	1.10	1.87	-	-

[1]: Colours and photometry from UKIDSS (Hewett et al. 2006), [2]: Colours and photometry from SDSS (Fukugita et al. 1996). Original discovery paper: [a]Geballe et al. (2002), [b]Hawley et al. (2002), [c]Burningham et al. (2010a), [d]Knapp et al. (2004), [e]Lodieu et al. (2007a), [f]Chiu et al. (2006), [g]Scholz (2010), [h]Burningham et al., in prep.

instrument+atmosphere response curve; finally the target spectra is multiplied by the response curve obtained to flux calibrate it. The arms (VIS and NIR) were then merged by matching the flux level in the overlapping regions between them. The flux calibration was checked by determining the target's synthetic MKO $YJHK$ magnitudes, that were compared to those obtained in the ULAS. Finally, each spectrum was visually inspected to check for possible problems during the extraction or merging stage. The spectra were then binned (in the λ direction) by 40 times to produce an average S/N= 30 for resolution R= 880 and 510 in the VIS and NIR arms, respectively.

5 SPECTROSCOPY

5.1 Spectral Types

Spectral types were determined via spectral fitting with template objects. Template spectra were obtained from the SpeX Prism Spectral Library [1], which are shown in Table. 3. Our observed spectra were then re-sampled to the same resolution as the SpeX data (see Table. 3) and spectral types were determined from the best chi-squared fit

[1] http://pono.ucsd.edu/ adam/browndwarfs/spexprism/

Table 2. Optical and near-infrared spectroscopic observations of sub-sample.

Name	UT date	VIS t_{int}(s)	VIS S/N*	NIR t_{int}(s)	NIR S/N*
BRLT1	19-Sep-2011	1600	4.54	1960	29.7
BRLT2	20-Sep-2011	2000	4.72	2360	18.8
BRLT3	28-Nov-2010	1200	5.21	1560	32.8
BRLT6	18-Sep-2011	2000	5.32	2360	25.2
BRLT7	20-Sep-2011	1600	7.61	1960	20.9
BRLT8	21-Sep-2011	1600	5.18	1960	31
BRLT9	19-Sep-2011	1600	8.01	1960	30.7
BRLT10	29-Nov-2010	800	2.39	1160	26.5
BRLT12	21-Sep-2011	2000	4.3	2360	18.7
BRLT14	30-Nov-2010	1600	7.56	1960	29.8
BRLT15	20-Sep-2011	1600	2.4	1960	21.6
BRLT16	28-Nov-2010	1400	3.66	1760	22.8
BRLT18	30-Nov-2010	1600	5.79	1960	29
BRLT20	21-Sep-2011	2000	5.12	2360	20.7
BRLT21	19-Sep-2011	1200	3.73	800	29.5
BRLT22	21-Sep-2011	1600	5.84	1960	17.7
BRLT24	21-Sep-2011	1600	4.17	1960	23.9
BRLT26	27-Nov-2010	600	4.14	600	24.2
BRLT27	29-Nov-2010	1600	2.22	1960	27.6
BRLT30	28-Nov-2010	800	6.39	1160	53.3
BRLT31	18-Sep-2011	2000	6.18	2360	27.6
BRLT32	20-Sep-2011	2000	5.76	2360	25
BRLT33	19-Sep-2011	1600	2.93	1960	20.9
BRLT35	21-Sep-2011	1600	5.86	1960	21.6
BRLT37	18-Sep-2011	2000	4.84	2360	26
BRLT38	27-Nov-2010	240	4.14	600	31.9
BRLT39	18-Sep-2011	1600	7.77	1960	29.8
BRLT42	20-Sep-2011	1600	5.75	1960	23.6
BRLT44	30-Nov-2010	1600	4.3	1960	28.6
BRLT45	21-Sep-2011	1600	3.76	1960	16.7
BRLT46	30-Nov-2010	1600	3.84	1960	21.6
BRLT48	28-Nov-2010	1400	2.93	1760	27.6
BRLT50	30-Nov-2010	2400	$\sim$1	2760	7.26
BRLT51	19-Sep-2011	2000	4.59	2360	22.9
BRLT52	27-Nov-2010	1200	6.55	1200	29.1
BRLT56	29-Nov-2010	1600	3.01	1960	22.8
BRLT57	30-Nov-2010	2400	3.93	2760	26.6
BRLT58	27-Nov-2010	1200	5.09	1200	27.1
BRLT60	25-Feb-2011	1400	4.11	1760	27.9
BRLT62	29-Nov-2010	1600	2.64	1960	26.8
BRLT64	27-Nov-2010	1200	5.26	1200	29.5
BRLT66	27-Nov-2010	800	4.82	800	27.5
BRLT305	8-Jun-2011	1600	1.94	1960	19.3
BRLT306	7-Jun-2011	1600	1.71	1960	25.7
BRLT307	18-Sep-2011	2000	7.84	2360	27.2
BRLT311	19-Sep-2011	1600	2.93	1960	16.2
BRLT312	20-Sep-2011	2000	4.38	2360	22.9
BRLT313	25-Feb-2011	1600	6.34	1960	42
BRLT314	7-Jun-2011	1200	1.71	1560	28.2
BRLT315	19-Sep-2011	1600	4.96	1960	25.3
BRLT316	21-Sep-2011	2000	4.41	2360	20.3
BRLT317	28-Nov-2010	800	13.7	1160	77.1
BRLT318	18-Sep-2011	1600	4.91	1960	21.7
BRLT320	20-Sep-2011	1600	4.49	1960	19.7
BRLT321	8-Jun-2011	1600	1.26	1960	16
BRLT322	18-Sep-2011	1600	5.48	1960	27.7
BRLT323	29-Nov-2010	800	3.83	1160	37.8
BRLT325	19-Sep-2011	1600	2.39	1960	18
BRLT328	29-Nov-2010	1600	4.23	1960	23.4

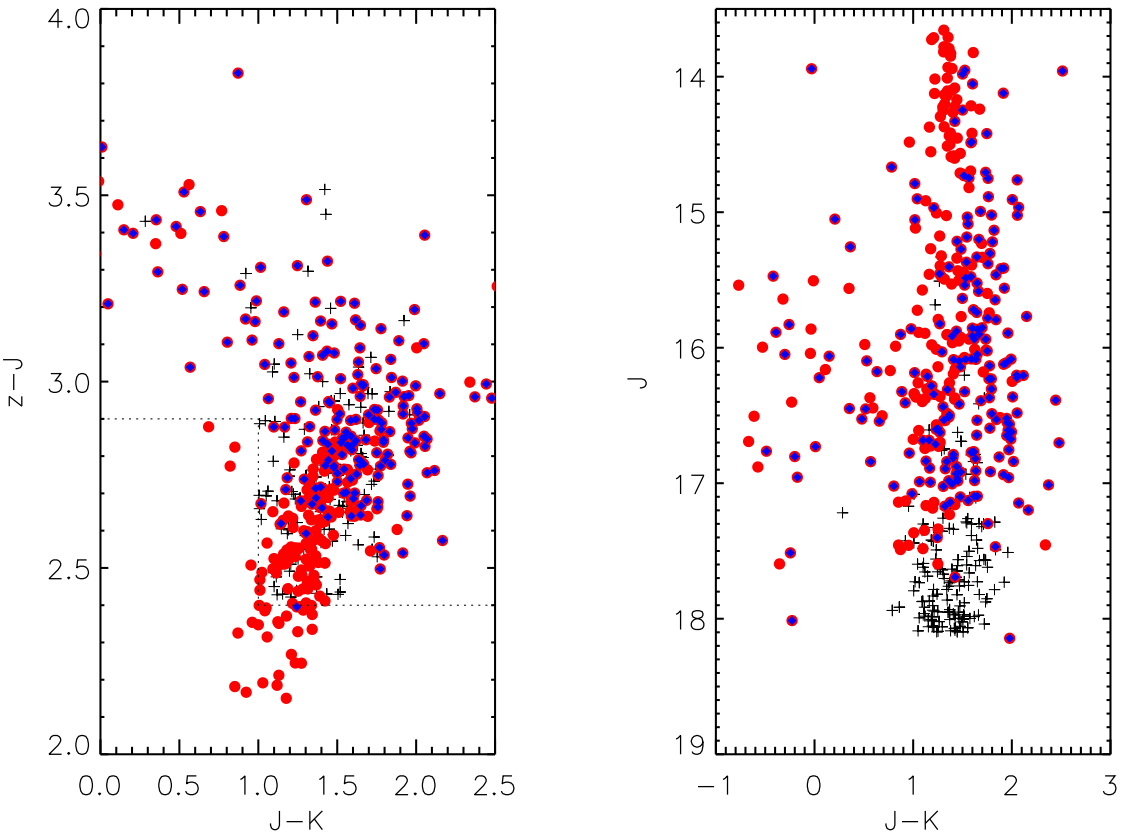

Figure 2. Left: Colour-colour diagram of candidate L and T dwarfs (crosses). Right: Colour-Magnitude diagram of candidate L and T dwarfs (crosses). Known L and T dwarfs (L0-T9) from Dwarfarchives.org are shown as filled red circles. Those with spectral types L3-T5 dwarfs are shown as small blue diamonds. Photometry is on the UKIDSS and SDSS system. Objects with 2MASS photometry have been converted using the colour conversions of Warren, Dye & Hambly (2006).

Table 2 continued. Optical and near-infrared spectroscopic observations of sub-sample.

BRLT330	20-Sep-2011	1600	5.2	1960	20.6
BRLT331	19-Sep-2011	2000	5.45	2360	21.9
BRLT332	18-Sep-2011	2000	7.87	2360	27.7
BRLT333	28-Nov-2010	800	1.7	1160	21.5
BRLT334	27-Oct-2010	240	4.06	600	33.9
BRLT335	21-Sep-2011	2000	3.75	2360	24.5
BRLT338	27-Nov-2010	800	3.44	800	18.2
BRLT343	28-Nov-2010	1200	3.67	1560	28
BRLT344	18-Sep-2011	2000	4.17	2360	26.8

*S/N is per spectral pixel, after binning.

to the templates using the spectral typing scheme from Kirkpatrick et al. (1999) and Burgasser et al. (2006), for L and T dwarfs, respectively. The three best fits were also visually inspected to make sure that they were good fits to the real spectra. The spectral types, as well as their associated errors are shown in Table. 4 and the spectra can be seen in ascending spectral type in Fig. 3 - 9.

5.2 Unresolved binarity

The L-T transition region is thought to be hindered with a substantial number of unresolved binaries (up to 45%; Maxted & Jeffries 2005), such that in order to measure a reliable formation history we must distinguish between these binaries. With the wavelength coverage of our X-shooter data we should be able to differentiate between binaries where the components are separated by more than 1 spectral type, leaving only the equal spectral-type binaries, which should not affect the overall shape of the $T_{\rm eff}$ distribution, since the equal $T_{\rm eff}$ binary fraction should be uniform over this spectral type range (Geißler et al. 2011).

We select potential binary candidates using the spectral indices and the criteria defined in Burgasser et al. (2010) who use index-index and index-spectral type combinations

Table 3. Spectral templates from the SpeX Prism Spectral Library used for spectral typing.

Object Name	2MASS Designation	Optical SpT	NIR SpT	Resolution	Reference
VB 8	J16553529-0823401	M7 V	M7	120	1
VB 10	J19165762+0509021	M8 V	M8	120	2
LHS 2924	J14284323+3310391	M9 V	M9	120	3
2MASSW J2130446-084520	J21304464-0845205	L1.5	L1	120	4
Kelu-1	J13054019-2541059	L2	L2	120	5
2MASSW J1506544+132106	J15065441+1321060	L3	L3	120	6
2MASS J21580457-1550098	J21580457-1550098	L4	L4	120	4
SDSS J083506.16+195304.4	J08350622+1953050	-	L5	120	7
2MASSI J1010148-040649	J10101480-0406499	L6	L6	120	8
2MASSI J0103320+193536	J01033203+1935361	L6	L7	120	9
2MASSW J1632291+190441	J16322911+1904407	L8	L8	75	5
DENIS-P J0255-4700	J02550357-4700509	L8	L9	120	10
SDSS J120747.17+024424.8	J12074717+0244249	L8	T0	120	11
SDSS J015141.69+124429.6	J01514155+1244300	-	T1	120	12
SDSSp J125453.90-012247.4	J12545393-0122474	T2	T2	120	12
2MASS J12095613-1004008	J12095613-1004008	T3.5	T3	120	12
2MASSI J2254188+312349	J22541892+3123498	-	T4	120	12
2MASS J15031961+2525196	J15031961+2525196	T6	T5	120	12
SDSSp J162414.37+002915.6	J16241436+0029158	-	T6	120	13
2MASSI J0727182+171001	J07271824+1710012	T8	T7	120	13
2MASSI J0415195-093506	J04151954-0935066	T8	T8	120	12

1: Burgasser et al. (2008), 2: Burgasser (2004), 3: Burgasser & McElwain (2006), 4: Kirkpatrick et al. (2010), 5: Burgasser (2007), 6: Burgasser et al. (2007), 7: Chiu et al. (2006), 8: Reid et al. (2006), 9: Cruz et al. (2004), 10: Burgasser et al. (2010), 11: Looper, Kirkpatrick & Burgasser (2007), 12: Burgasser (2004), 13: Burgasser et al. (2006)

Table 5. Binary indices as defined by Burgasser et al. (2006), except for H-dip, which is defined by Burgasser et al. (2010).

Index	Numerator Range	Denominator Range	Feature
H_2O-J	1.14-1.165	1.26-1.285	1.15 μm H_2O
H_2O-H	1.48-1.52	1.56-1.60	1.4 μm H_2O
H_2O-K	1.975-1.995	2.08-2.10	1.9 μm H_2O
CH_4-J	1.315-1.34	1.26-1.285	1.32 μm CH_4
CH_4-H	1.635-1.675	1.56-1.60	1.65 μm CH_4
CH_4-K	2.215-2.255	2.08-2.12	2.2 μm CH_4
K/J	2.060-2.10	1.25-1.29	J-K colour
H-dip	1.61-1.64	1.56-1.59 + 1.66-1.69	1.65 μm CH_4

Table 6. Inflection points used for analysis of unresolved binarity Burgasser et al. (2010).

Abscissa	Ordinate	Inflection Points (x,y)
H_2O-J	H_2O-K	(0.325,0.5),(0.65,0.7)
CH_4-H	CH_4O-K	(0.6,0.35),(1,0.775)
CH_4-H	K/J	(0.65,0.25),(1,0.375)
H_2O-H	H-dip	(0.5,0.49),(0.875,0.49)
SpT	H_2O-J/H_2O-H	(L8.5,0.925),(T1.5,0.925),(T3.5,0.85)
SpT	H_2O-J/CH_4-K	(L8.5,0.625),(T4.5,0.825)

to define six different criteria to segregate possible unresolved L-T transition binaries, using known double objects as reference. These spectral indices take into account the flux ratio of the prominent molecular absorption bands of water and methane over the flux emitted in the J, H and K bands. Objects that match two criteria are called weak candidates while objects that match at least three of them are called strong candidates. For clarity, all criteria used to classify these dwarfs are re-stated in Table. 5 and 6. We show our observed sample and the binary selection criteria applied in the different index-index and index-spectral type in Fig. 10. In this way we identified six strong candidates and six weak candidates, which are highlighted as diamonds and asterisks, respectively.

The 12 unresolved binary candidates were investigated further using synthetic binary template fitting. The synthetic binaries were created by taking the standard spectral type templates available in the SpeX-Prism library. These were then normalized to 1 at 1.28μm and scaled the spectra to an absolute flux level, using the absolute J magnitude - spectral type relation derived in Marocco et al. (2010). Finally all the templates were combined to make our own set of synthetic unresolved binaries. We then performed a chi-squared fit of our spectra to the templates. The results of the fitting are presented in Table. 5.2, with the best-fitting combined template over-plotted on the spectra of the 12 binary candidates shown in Fig. 11 and 12. For each object we list the best fit single object template and the associated chi-squared, the best fit combined template and its associated chi-squared fit value. The results of the two fits were compared using a one-sided F test to assess their statistical significance. If the ratio of the two chi-squared fits (η) is greater than the critical value (1.15), this represents a 99% significance that the combined template fit is better than the standard template alone. The last column of Table 5.2 presents the results of the F test, where it can be seen that six of the 12 candidates give statistically better fits using

Table 4. Spectral details of observed targets.

ID	Spectral type	H_2O-J	H_2O-H	H_2O-K	CH_4-J	CH_4-H	CH_4-K	K/J	H-dip	Notes
BRLT1	L9.0 ± 0.5	0.72	0.68	0.86	0.75	1.00	0.76	0.60	0.49	
BRLT2	L1.0 ± 1.0	0.94	0.76	1.13	0.80	1.09	1.06	0.40	0.46	
BRLT3	L9.0 ± 1.0	0.75	0.69	0.87	0.73	1.04	0.90	0.58	0.50	
BRLT6	L3.0 ± 1.0	0.85	0.82	1.04	0.83	1.13	1.11	0.45	0.49	
BRLT7	M8.0 ± 1.0	0.95	0.87	1.15	0.86	0.98	0.91	0.36	0.50	
BRLT8	L8.5 ± 0.5	0.71	0.75	0.87	0.77	1.03	0.89	0.67	0.49	
BRLT9	L1.0 ± 1.0	0.95	0.84	0.98	0.86	1.03	0.95	0.36	0.48	
BRLT10	L9.0 ± 0.5	0.67	0.72	0.79	0.76	1.05	0.85	0.64	0.52	
BRLT12	L3.0 ± 1.0	0.75	0.76	0.95	0.74	1.05	0.99	0.45	0.47	
BRLT14	L0.0 ± 0.5	0.97	0.84	1.13	0.86	1.05	1.05	0.37	0.48	
BRLT15	T2.0 ± 2.0	0.49	0.63	0.81	0.57	0.92	0.75	0.52	0.47	SC
BRLT16	L3.5 ± 0.5	0.90	0.75	0.96	0.83	0.93	0.95	0.42	0.45	WC
BRLT18	L0.0 ± 1.0	1.03	0.91	1.02	0.94	1.03	0.95	0.39	0.49	
BRLT20	L1.0 ± 1.0	0.87	0.76	1.00	0.76	0.99	0.91	0.32	0.47	
BRLT21	L3.5 ± 0.5	0.83	0.75	0.95	0.80	1.00	0.98	0.45	0.47	
BRLT22	M9.5 ± 0.5	1.01	0.90	1.16	0.87	1.12	0.86	0.32	0.51	
BRLT24	L3.5 ± 0.5	0.80	0.74	0.96	0.80	1.00	0.97	0.47	0.46	
BRLT26	L5.5 ± 0.5	0.80	0.72	0.91	0.81	1.07	0.96	0.53	0.48	
BRLT27	T1.0 ± 0.5	0.62	0.64	0.78	0.63	1.01	0.59	0.40	0.50	
BRLT30	L5.0 ± 0.5	0.74	0.75	0.95	0.79	1.08	1.01	0.51	0.48	
BRLT31	L4.0 ± 1.0	0.74	0.69	0.92	0.77	1.01	0.85	0.51	0.50	
BRLT32	L1.5 ± 0.5	0.85	0.79	1.08	0.83	1.04	1.05	0.40	0.48	
BRLT33	L3.5 ± 0.5	0.82	0.73	0.90	0.80	0.94	0.91	0.45	0.47	WC
BRLT35	M9.5 ± 0.5	1.01	0.85	1.00	0.93	1.04	1.00	0.41	0.48	
BRLT37	L5.0 ± 0.5	0.71	0.71	0.82	0.76	1.09	0.93	0.53	0.50	
BRLT38	T1.0 ± 0.5	0.65	0.65	0.77	0.68	0.95	0.67	0.40	0.51	
BRLT39	L5.0 ± 1.0	0.79	0.75	0.93	0.77	1.04	0.95	0.46	0.50	
BRLT42	M9.0 ± 0.5	1.04	0.89	1.10	0.95	0.94	0.94	0.45	0.47	WC
BRLT44	L5.0 ± 1.0	0.72	0.75	0.83	0.74	1.00	0.81	0.52	0.49	
BRLT45	T1.0 ± 0.5	0.57	0.61	0.71	0.64	0.88	0.57	0.42	0.47	SC
BRLT46	L0.5 ± 0.5	0.91	0.76	1.13	0.80	1.12	1.07	0.30	0.48	
BRLT48	L4.5 ± 0.5	0.77	0.77	1.04	0.81	1.19	1.08	0.55	0.49	
BRLT50	T7.0 ± 0.5	0.16	0.33	0.84	0.28	0.25	-0.0	0.06	0.20	
BRLT51	L3.0 ± 1.0	0.80	0.78	0.86	0.83	1.06	0.92	0.51	0.47	
BRLT52	L5.5 ± 0.5	0.75	0.68	0.94	0.77	1.05	0.94	0.57	0.50	
BRLT56	L1.5 ± 1.0	0.91	0.86	0.93	0.85	1.01	0.96	0.44	0.49	
BRLT57	L0.0 ± 1.0	0.97	0.86	1.08	0.84	1.09	0.99	0.37	0.50	
BRLT58	L5.5 ± 1.0	0.76	0.72	0.84	0.74	1.05	1.01	0.41	0.49	
BRLT60	L1.0 ± 1.0	0.83	0.79	0.99	0.84	0.99	0.94	0.41	0.46	WC
BRLT62	L5.0 ± 1.0	0.83	0.76	0.97	0.86	1.11	1.04	0.63	0.49	
BRLT64	L4.0 ± 0.5	0.76	0.73	0.92	0.83	1.05	1.01	0.50	0.48	
BRLT66	L5.0 ± 0.5	0.74	0.69	0.92	0.79	1.08	0.95	0.52	0.48	
BRLT305	L5.5 ± 1.0	0.93	0.79	0.95	0.91	0.97	0.93	0.61	0.47	WC
BRLT306	L4.5 ± 1.0	0.81	0.80	0.95	0.75	1.01	0.92	0.39	0.48	
BRLT307	L1.0 ± 0.5	0.92	0.89	1.17	0.93	1.07	0.93	0.47	0.48	
BRLT311	T3.0 ± 0.5	0.42	0.56	0.78	0.55	0.70	0.57	0.29	0.44	SC
BRLT312	T0.0 ± 0.5	0.62	0.67	0.87	0.66	0.92	0.90	0.44	0.42	SC
BRLT313	L3.5 ± 0.5	0.82	0.74	0.94	0.88	1.04	0.99	0.53	0.47	
BRLT314	L7.5 ± 0.5	0.72	0.71	0.88	0.80	1.05	0.95	0.69	0.49	
BRLT315	L1.0 ± 1.0	0.87	0.82	0.92	0.78	1.04	1.01	0.35	0.47	
BRLT316	L1.0 ± 0.5	0.87	0.87	0.91	0.81	1.13	0.98	0.35	0.49	
BRLT317	L1.0 ± 1.0	0.79	0.71	0.92	0.70	1.09	0.95	0.31	0.49	
BRLT318	L1.0 ± 0.5	0.83	0.88	0.97	0.85	1.13	0.95	0.42	0.49	
BRLT320	L1.0 ± 0.5	0.89	0.79	0.90	0.85	1.10	0.89	0.42	0.50	
BRLT321	T4.0 ± 0.5	0.37	0.42	0.57	0.43	0.60	0.25	0.24	0.37	
BRLT322	L5.0 ± 0.5	0.71	0.70	0.90	0.72	1.07	0.90	0.55	0.52	
BRLT323	T0.0 ± 1.0	0.76	0.71	0.87	0.76	1.04	1.04	0.42	0.49	
BRLT325	T2.0 ± 1.0	0.53	0.47	0.63	0.55	0.89	0.49	0.27	0.48	
BRLT328	L0.5 ± 1.0	0.89	0.78	0.97	0.82	1.09	1.05	0.36	0.50	

Table 4 continued. Spectral details of observed targets.

ID	Spectral type	H_2O-J	H_2O-H	H_2O-K	CH_4-J	CH_4-H	CH_4-K	K/J	H-dip	Notes
BRLT330	L1.0 ± 1.0	0.81	0.77	0.89	0.73	1.20	0.95	0.35	0.48	
BRLT331	L1.0 ± 2.0	0.84	0.71	1.06	0.74	1.05	0.93	0.30	0.49	
BRLT332	L2.0 ± 2.0	0.87	0.85	1.00	0.75	1.10	0.96	0.34	0.49	
BRLT333	T2.0 ± 0.5	0.52	0.57	0.77	0.59	0.98	0.72	0.38	0.52	SC
BRLT334	L3.5 ± 0.5	0.83	0.74	0.91	0.82	1.04	0.95	0.48	0.48	
BRLT335	L4.0 ± 1.0	0.81	0.74	0.95	0.79	0.99	0.92	0.42	0.47	WC
BRLT338	L1.0 ± 1.0	0.88	0.73	1.01	0.81	1.09	1.12	0.34	0.49	
BRLT343	L9.0 ± 1.0	0.69	0.70	0.88	0.75	1.05	0.92	0.60	0.49	
BRLT344	T0.0 ± 1.0	0.54	0.68	0.96	0.68	0.94	0.89	0.54	0.44	SC

SC=Strong binary candidate, WC=Weak binary candidate

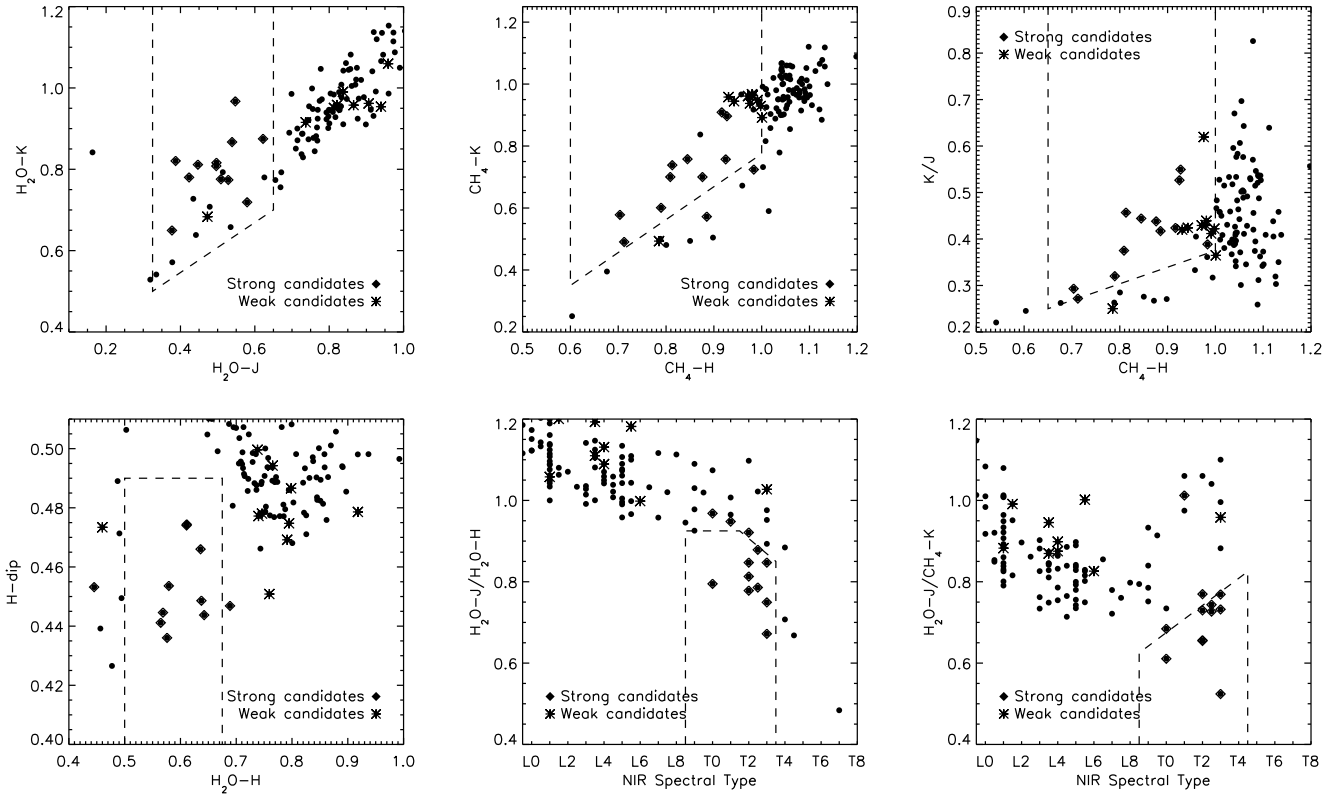

Figure 10. Index-Index plots showing the selection criteria applied for unresolved binary candidate segregation. Strong and weak candidates are marked as diamonds and crosses respectively.

the combined templates, such that they are the strongest binary candidates. It should be noted that the results of this fitting are not conclusive (Burgasser et al. 2010), and the real nature of these objects must be investigated further using adaptive optics imaging or spectro-astrometry in order to confirm or not their true binary nature.

6 CONSTRAINING THE GALACTIC BROWN DWARF FORMATION HISTORY

In order to compare the findings from our first sub-sample of 76 mid L to mid T dwarfs that occupy a complete area of 495 sq degrees of sky (RA=22 to 4 hr and DEC=-2 to 16 deg) down to a magnitude limit of J=18.1, with the results from simulations of differing birth rates, we constructed a space density vs spectral type/$T_{\rm eff}$ histogram. We firstly calculated the space density of our targets by converting their spectral types into effective temperatures using the $T_{\rm eff}-$ NIR spectral type relation presented in Stephens et al. (2009, equation 3). Using a bin sizes of 1700-1450K, 1150-1300K and 1300-1450K (corresponding to bins in spectral type of L4-L6, L7-T0 and T1-T4), we calculated for each bin the maximum distance at which an object could have been selected using the M_J- NIR spectral type relation from Marocco et al. (2010). With this distance limit we then calculated the volume sampled by each $T_{\rm eff}$ bin. The derived space densities were then corrected for Malmquist and Eddington bias following the approach described in Pinfield et al. (2008). The Eddington bias is caused by the photometric uncertainties

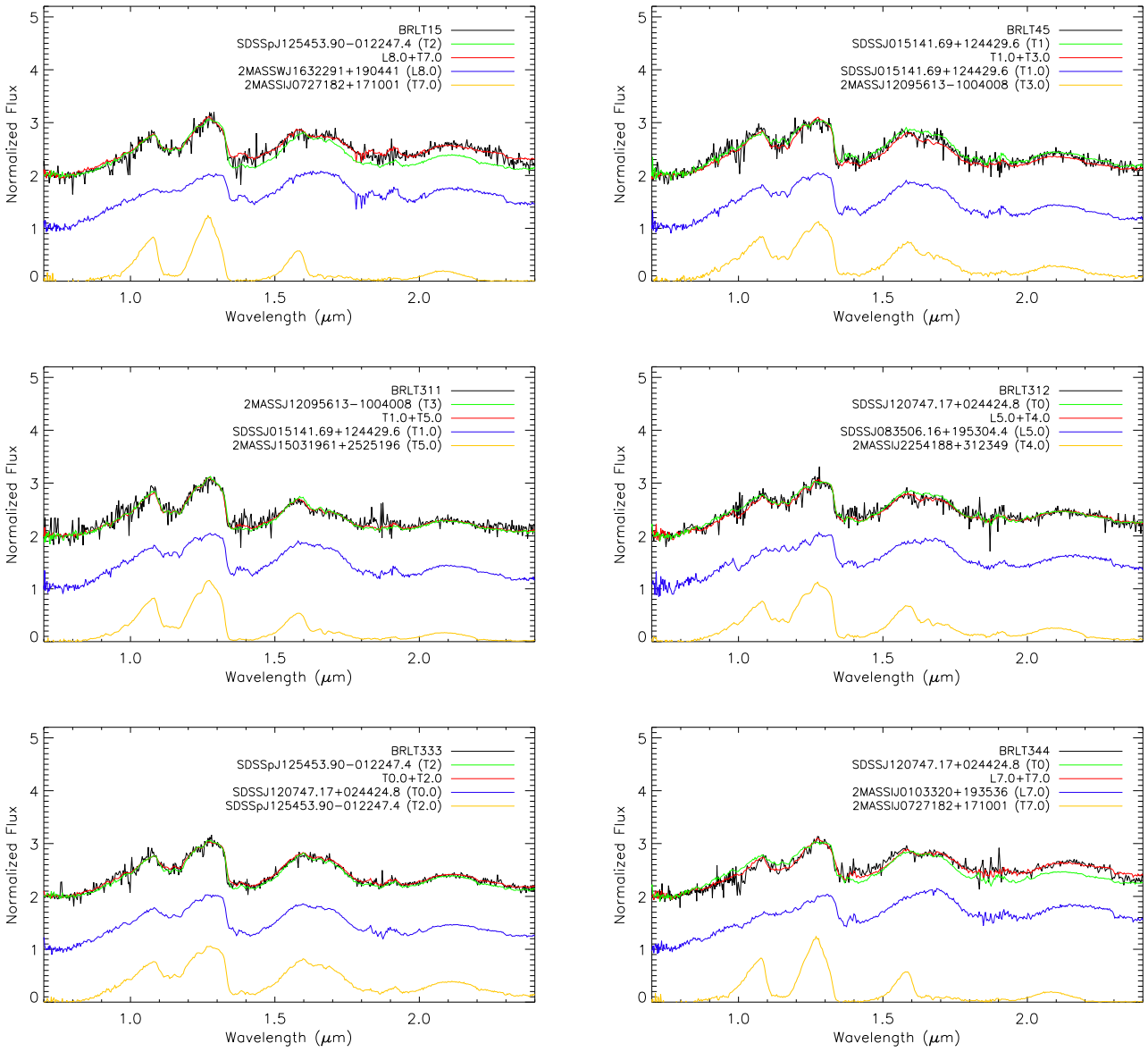

Figure 11. "Strong" unresolved binary candidates over-plotted with combined spectral templates.

on the magnitudes of objects near our cut (i.e. J < 18.1). However, since the magnitude cut we impose is bright (it corresponds to a $\sim 12\sigma$ detection in the UKIDSS LAS), the uncertainties at the J=18.1 limit are typically less than σ=0.05 and therefore the Eddington bias correction is less than 1%. This is negligible compared to the other sources of uncertainty. We estimated the Malmquist bias correction considering the mean scatter of the sample of known L and T dwarfs around the adopted M_J- NIR spectral type relation. This represents an increase in the volume sampled of 22%.

6.1 Completeness

In order to calculate the completeness of our sample we compared it to a control sample of known L and T dwarfs taken from DwarfArchives.org, for a magnitude limit of $J \leqslant 16$, removing any objects that are known to be members of unresolved binary systems. The control sample was cross matched with the UKIDSS LAS and SDSS in order to obtain photometry on the same colour system as our selection criteria. We use DR9 of the UKIDSS LAS and DR8 of the SDSS in order to get a sufficiently large control sample. We imposed the same set of colour cuts, as described in §3 to reveal the level of completeness of our sample selection. We retain all of the L4 dwarfs from the control sample, but only some of the L0-L3 dwarfs when imposing our colour cuts, as such we find that our sample selection is complete for L4 spectral types and later.

We also consider how many objects we may lose from our selection due to photometric scattering of colours. We calculate that for L0-L3 types we would expect to lose 3.7 dwarfs, this corresponds to a completeness level of 85% for L0-L3 dwarfs due to photometric scatter, although we note

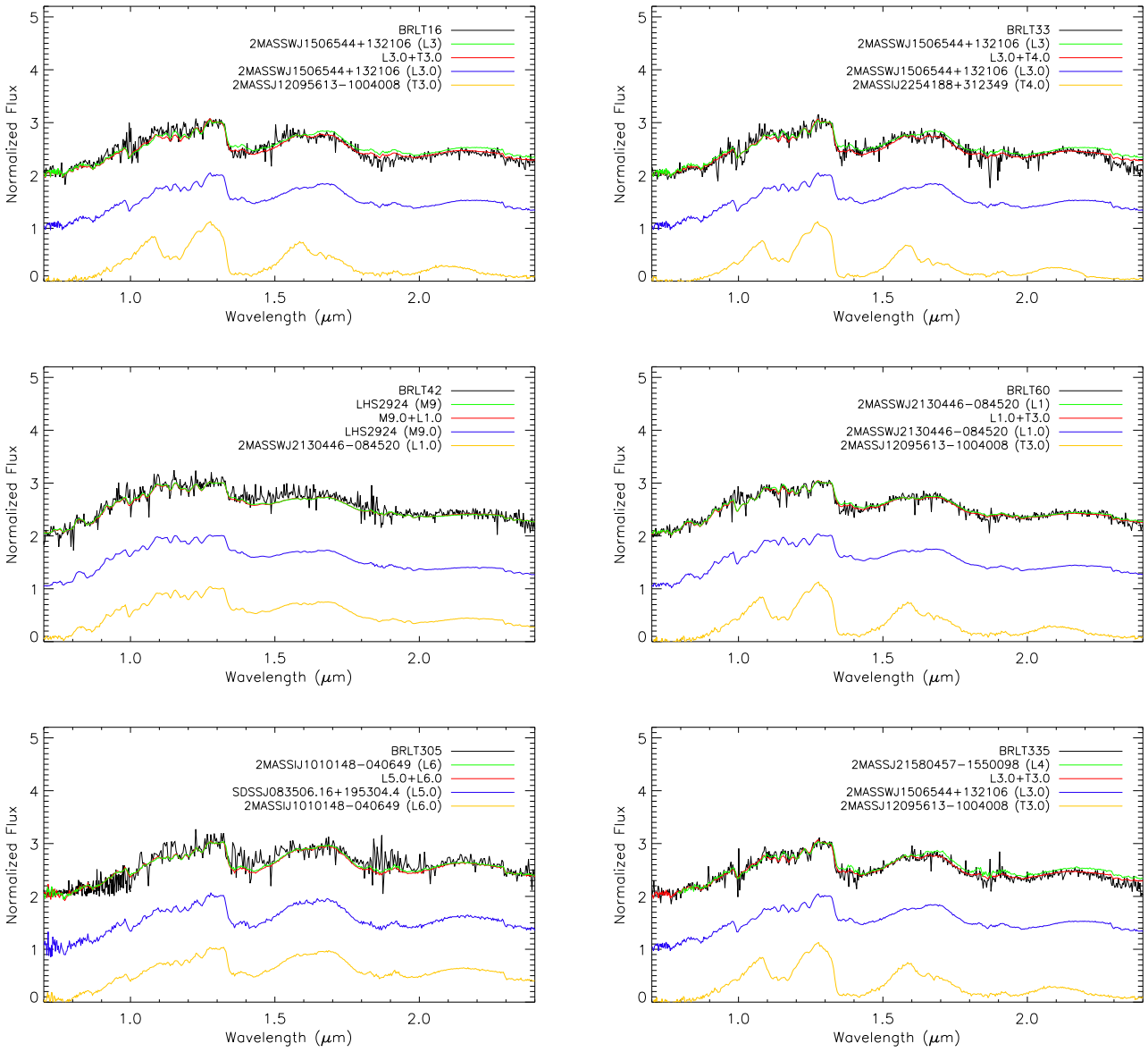

Figure 12. " Weak" unresolved binary candidates over-plotted with combined spectral templates.

that we are significantly incomplete from our colour selection for this spectral range. For L4-L6 dwarfs we would expect to lose 2.33 dwarfs, being 88% complete. The L7-T0 range would lose 0.55 dwarfs, corresponding to a 94% completeness; and for T1-T4 we would expect to lose 0.05 dwarfs, corresponding to a completeness of 99%.

We combine the completeness for colour selection, colour scatter as well as the Malmquist and Eddington biases to infer a 90% completeness for the $T_{\rm eff}$ =1450-1700K and 97% for the $T_{\rm eff}$=1300-1450K and 97% for the $T_{\rm eff}$=1150-1300K range in our sample.

6.2 Correction for unresolved binarity

We also corrected our results for the presence of binaries by firstly removing objects identified as possible binaries (§5.2) for which our spectral deconvolution gives a statistically better fit. We then applied a further correction to take into account the presence of equal spectral type binaries, which would fall beyond our J < 18.1 limit if they were single objects, using the definition of "observed binary fraction" given by Burgasser et al. (2003), such that:

$$\frac{N_B}{N_m} = \frac{\gamma + 1}{BF - 1} \quad (1)$$

where N_B and N_m are the observed binaries and the total number of objects respectively, BF is the "true" binary fraction, and γ is the fractional increase in volume due to inclusion of binaries in the sample. The number of binaries that fall within our magnitude limit (N_D) is:

$$\frac{N_D}{N_B} = \frac{\gamma - 1}{\gamma} \quad (2)$$

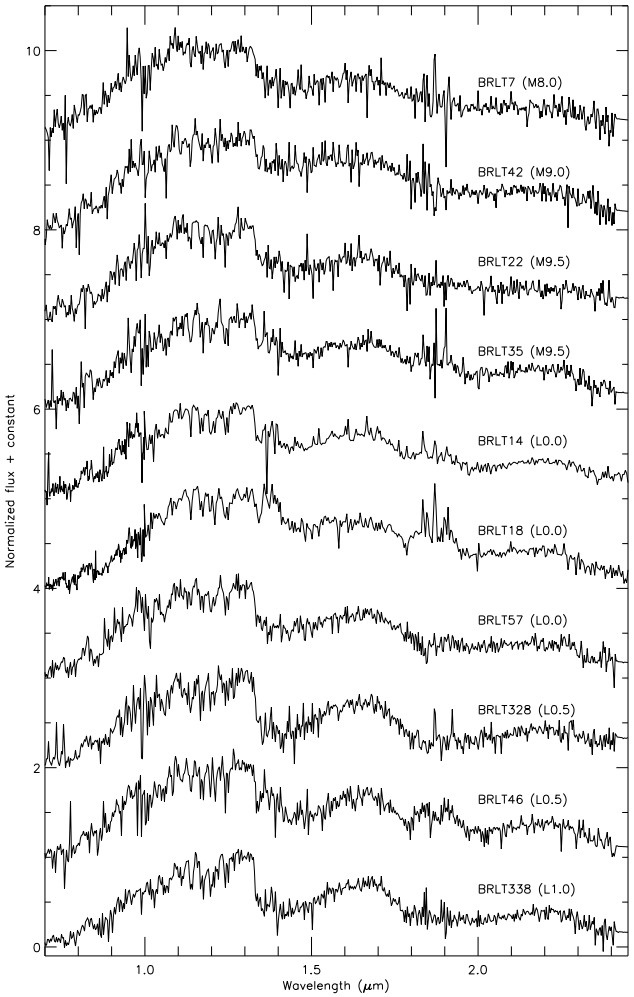

Figure 3. X-shooter spectra of L and T dwarfs from birth rate sample, in ascending spectral type.

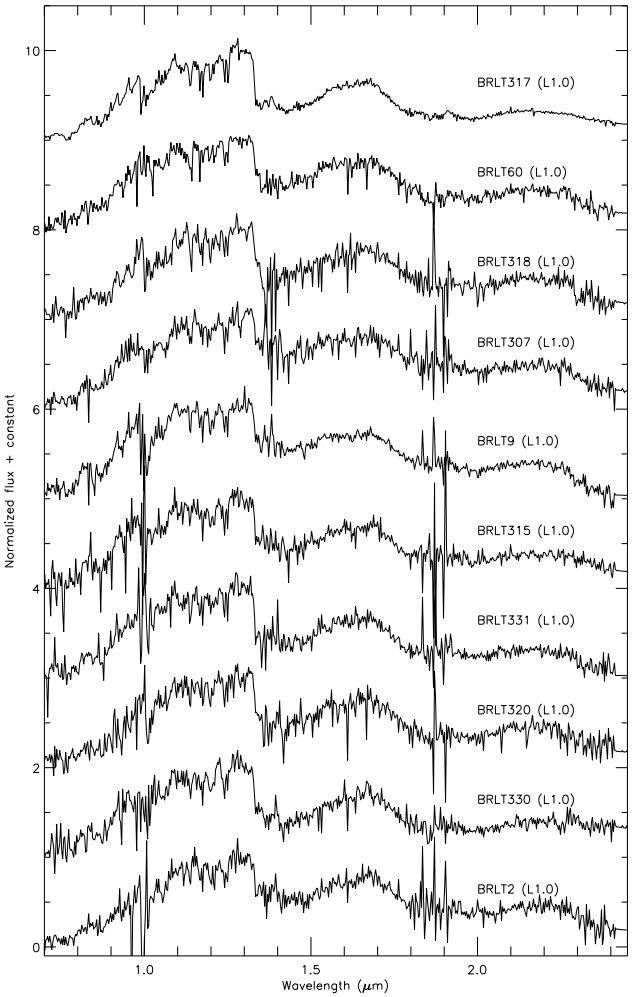

Figure 4. X-shooter spectra of L and T dwarfs from birth rate sample, in ascending spectral type.

Table 7. Results of spectral fitting of binary candidates using combined templates.

Target ID	Single template best fit (χ^2)	Combined template best fit (χ^2)	F-test η
Strong candidates			
BRLT15	T2.0 (14.8341)	L8.0+T7.0 (3.6926)	4.02
BRLT45	T1.0 (6.2583)	T1.0+T3.0 (6.7607)	0.92
BRLT311	T3.0 (9.3321)	T1.0+T5.0 (7.2732)	1.28
BRLT312	T0.0 (6.5036)	L5.0+T4.0 (5.3935)	1.20
BRLT333	T2.0 (3.5947)	T0.0+T2.0 (3.7963)	0.95
BRLT344	T0.0 (5.8038)	L7.0+T7.0 (3.5877)	1.62
Weak candidates			
BRLT16	L3.5 (3.7444)	L3.0+T3.0 (3.6042)	1.04
BRLT33	L3.5 (6.0794)	L3.0+T4.0 (4.4195)	1.37
BRLT42	M9.0 (5.2356)	M9.0+L1.0 (3.3914)	1.54
BRLT60	L1.0 (2.2994)	L1.0+T3.0 (2.1760)	1.06
BRLT305	L5.5 (7.0290)	L5.0+L6.0 (8.9120)	0.79
BRLT335	L4.0 (4.6314)	L3.0+T3.0 (4.2767)	1.08

Therefore the fraction of objects to be excluded from our sample (f_{excl}) is

$$f_{excl} = \frac{N_B}{N_m}\frac{N_D}{N_B} = \frac{\gamma - 1}{\gamma + 1/BF - 1} \quad (3)$$

For equal spectral type binaries $\gamma = 2\sqrt{2}$. For the "true" binary fraction we assumed two extremes values taken from the literature. Following Burningham et al. (2010a), for the lower limit we considered the values obtained by Burgasser et al. (2003) who estimated a BF of 5-24% using AO imaging; for the upper limit we used the values given by Maxted & Jeffries (2005), who estimated a BF of 32-45% via radial velocity monitoring.

6.3 Space densities

We combine our calculated space densities, taking into account our completeness and contribution from unresolved binaries, with those from Burningham et al. (2010a) for late-type T dwarfs. We choose to use the Burningham et al. (2010a) space densities in favour of others available in the literature (e.g. Cruz et al. 2007, Metchev et al. 2008, Reylé et al. 2010, Kirkpatrick et al. 2012) as this is the

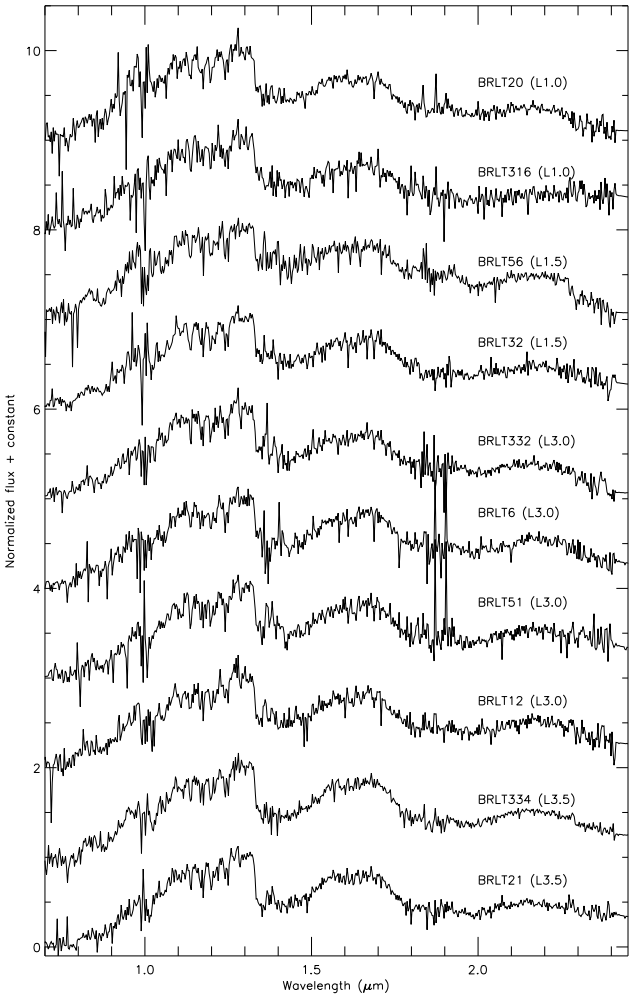

Figure 5. X-shooter spectra of L and T dwarfs from birth rate sample, in ascending spectral type.

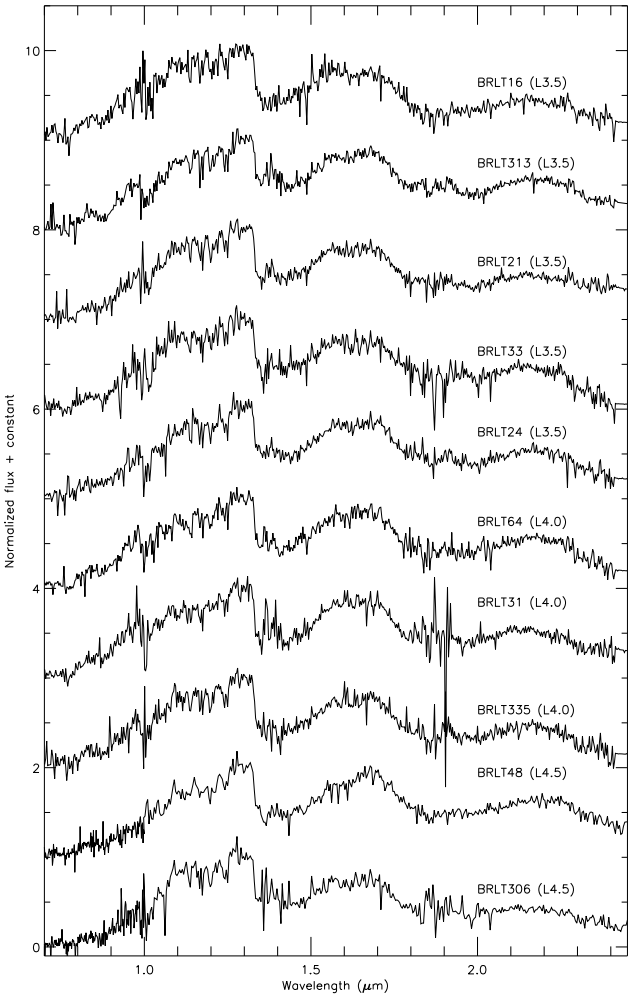

Figure 6. X-shooter spectra of L and T dwarfs from birth rate sample, in ascending spectral type.

only space density that can be used in direct comparison to our own sample, as we use the same M_J-spectral type relations as well as apply the same binary fractions. It is also probes down to a magnitude limit comparable to our sample. The Cruz et al. (2007) space densities only probe out to the 2MASS limit ($\sim J = 16$) and covers only M9-L8 dwarfs, and not the full range of spectral types we are probing. The Metchev et al. (2008) sample provide space densities obtained from 2MASS, combined with SDSS, and as such does not probe as deeply as our sample, or completely into the late T dwarf spectral type as that of Burningham et al. (2010a) . The Reylé et al. (2010) derived space densities could also be comparable but for their very late T type densities (T6-T8), they only have a handful of objects and do not make any correction for binarity. As such the Burningham et al. (2010a) space densities act as a complementary extension to our mid L-mid T derived space densities. Our calculated space densities are shown in Table.8, with comparison to the above mentioned published space densities for L and T dwarfs.

Our space densities are also shown as a function of both spectral type in Fig. 13, and as a function of $T_{\rm eff}$ in Fig. 14, where we show two points for each of our $T_{\rm eff}$/spectral type bin, the upper most points represent the density corresponding to a binary fraction of just 5%, while the lower points are those for a binary fraction of 45%. Also overplotted are space densities published for L and T dwarfs. In addition we show (overplotted) the results of numerical simulations computed assuming different IMF and birth rates. Details of the simulations are presented in Deacon & Hambly (2006) and are briefly summarized here.

We assume an exponential IMF in the form:

$$\psi(M) \propto M^{-\alpha} \ (pc^{-3}\mathrm{M}_{\odot}{}^{-1}). \quad (4)$$

where Ψ is the number of objects per unit volume in a given mass interval. We also assumed an exponential birth rate of the form:

$$b(t) \propto e^{-\beta t} \quad (5)$$

where t is in Gyr and β is the inverse of the scale time τ (in Gyr, since the galaxy was formed). Each simulated object was assigned an age based on the birth rate and a mass based on the IMF, giving a final creation function C given by the equation:

$$C(M,t) = \Psi(M)\frac{b(t)}{T_{\rm G}} \quad (6)$$

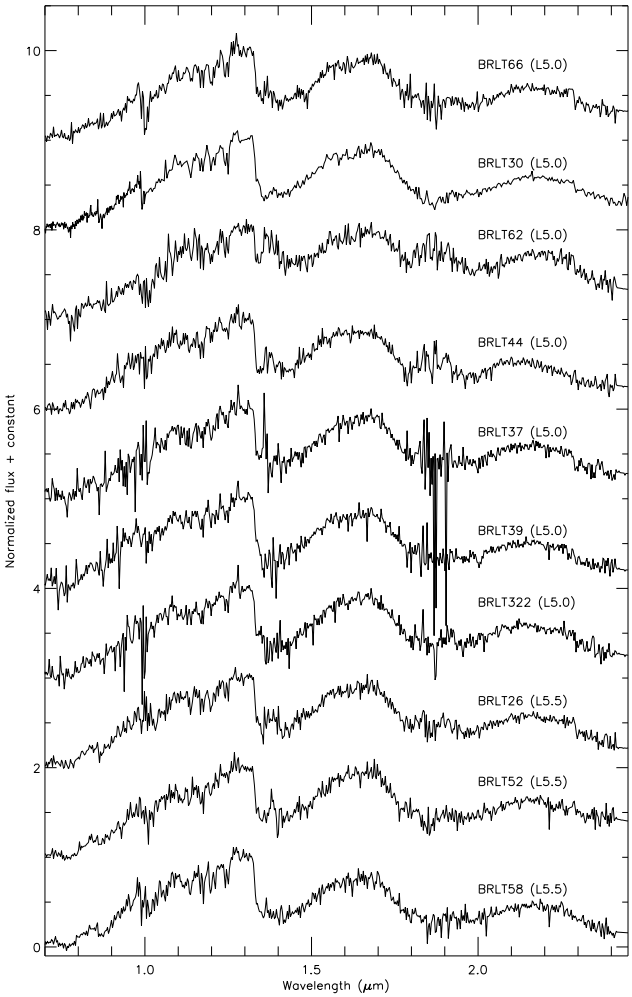

Figure 7. X-shooter spectra of L and T dwarfs from birth rate sample, in ascending spectral type.

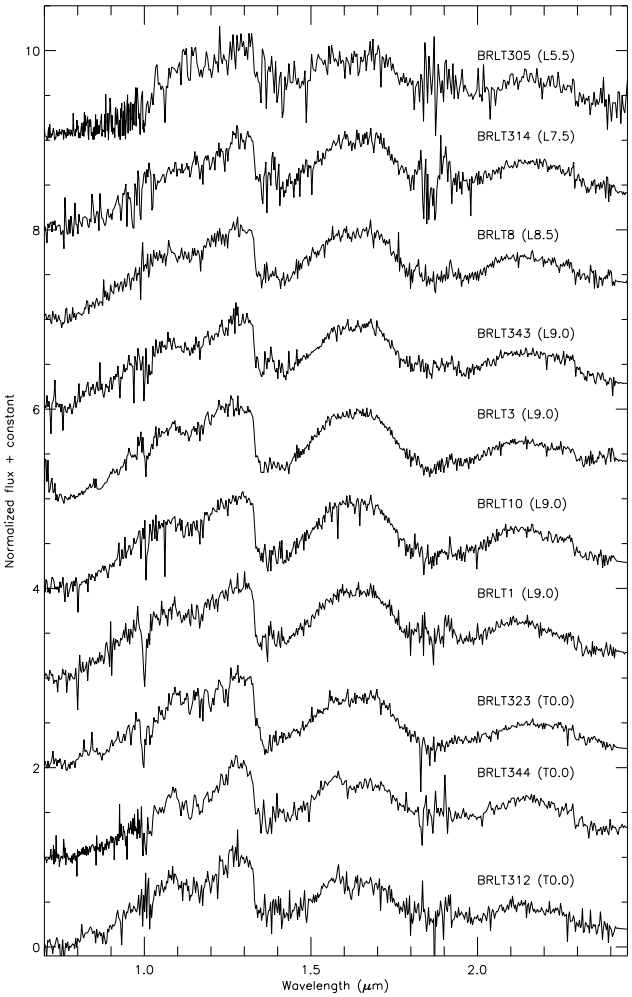

Figure 8. X-shooter spectra of L and T dwarfs from birth rate sample, in ascending spectral type.

where $T_{\rm G}$ is the age of the Galaxy. C is therefore the number of objects created per unit time per unit mass.

The evolution of each object and its parameters (i.e. $T_{\rm eff}$ and absolute magnitudes) were calculated using the evolutionary models from Baraffe et al. (2003). We note that any any model dependent systematics would be introduced, but that these should not effect the overall trend. The number densities obtained for each temperature bin were finally normalized to 0.0024 pc^{-3} in the 0.1−0.09 M$_{\odot}$ mass range, according to Deacon, Nelemans & Hambly (2008).

We consider five different values of β (-0.2,-0.1,0.0,+0.1,+0.2 corresponding to τ=-5,-10,∞,+10,+5 Gyr respectively) and five values of α (0.0,-0.5,-1.0-,1.5,-2.0). The results obtained for α = 0.0,-1.0,-2.0 and β = 0.0,0.2,0.5 are shown in Figure 14, where different colours represent different values of α and different line styles represent different values of β.

A first look at our measured mass function shows that the more extreme birth rates (e.g. a halo type form) can likely be excluded as the true form of the birth rate. Our space densities are in general agreement with the previous Bayesian analysis of 2MASS L and T dwarfs by Allen et al. (1995), and do not differ drastically (within our uncertainties) from those mass functions previously measured and discussed earlier (i.e. Cruz et al. 2007; Metchev et al. 2008; Reylé et al. 2010; Burningham et al. 2010a; Kirkpatrick et al. 2012). The differences between our derived densities and those previously published can be accounted for in large due to the use of different M$_J$-SpT conversions by the different groups.

Our space densities do however suggestive of a preference for an $\alpha < -1.0$, which is consistent with the studies of late T dwarfs alone from Pinfield et al. (2008) and Burningham et al. (2010a), where they conservatively find $\alpha < 0$. Indeed all three samples are indicative of an $-1 < \alpha < 0$. It can be seen however that it is not currently possible to place robust constraints on the birth rate with this sub-sample. One of the largest sources of uncertainties is the binary fraction. This could be resolved with the follow-up of our unresolved binary candidates, by either adaptive optics imaging or radial velocity. In addition improved numbers from the completion of follow-up of our full sample would allow us to place better constraints on the birth rate and would allow us to rule out at least $\beta = 0$ or $\beta = 0.5$ as the uncertainties are reduced. With spectroscopic

Table 8. Calculated space densities.

Reference	Sp. Type range	Space density (no correction) ($\times 10^{-3}$ pc^{-3})	Malmquist and Eddington bias correction (%)	Binary correction (%)	Space density ($\times 10^{-3}$ pc^{-3})
This paper	L4 - L6.5	0.345 ± 0.061	22	3-45	$0.176 \pm 0.031 - 0.295 \pm 0.052$
	L7 - T0.5	0.293 ± 0.050	22	3-45	$0.140 \pm 0.024 - 0.235 \pm 0.040$
	T1 - T4.5	0.235 ± 0.088	22	3-45	$0.106 \pm 0.040 - 0.178 \pm 0.067$
Burningham et al. (2010a)	T6 - T6.5	-	12-16	3-45	$0.30 \pm 0.2 - 0.59 \pm 0.39$
	T7 - T7.5	-	12-16	3-45	$0.40 \pm 0.28 - 0.79 \pm 0.55$
	T8 - T8.5	-	12-16	3-45	$0.58 \pm 051 - 1.1 \pm 1.0$
	T9	-	12-16	3-45	$3.1 \pm 2.9 - 6.1 \pm 5.7$
Reyle et al. (2010)	L5 - L9.5	-	-	-	$2.0^{+0.8}_{-0.7}$
	T0 - T5.5	-	-	-	$1.4^{+0.3}_{-0.2}$
	T6 - T8	-	-	-	$5.3^{+3.1}_{-2.2}$
Cruz et al. (2007)	M7 - M9.5	-	-	-	4.9 ± 0.6
	L0 - L3	-	-	-	1.7 ± 0.4
	L3.5 - L8	-	-	-	2.2 ± 0.4
Metchev et al. (2008)	T0 - T2.5	-	-	$\sim$50	$0.86^{+0.48}_{-0.44}$
	T3 - T5.5	-	-	$\sim$22	$1.4^{+0.8}_{-0.8}$
	T6 - T8	-	-	$\sim$14	$4.7^{+3.1}_{-2.8}$
Kirkpatrick et al. (2012)	T6 - T6.5	-	-	30	1.1
	T7 - T7.5	-	-	30	0.93
	T8 - T8.5	-	-	30	1.4
	T9 - T9.5	-	-	30	1.6
	Y0 - Y0.5	-	-	30	1.9

follow-up of a full sample the errors could be reduced by up to 50%.

7 SUMMARY

We have identified 63 new brown dwarfs that lie in the L-T transition region, including the identification of 12 possible unresolved binary systems. In order to confirm these as real binary systems additional adaptive optics/ radial velocity measurements are planned. We converted our 76 strong new sample onto a histogram of spatial density vs $T_{\rm eff}$/SpT and compared them with simulations of differing birth rates from Deacon & Hambly (2006). This showed that the mid L-mid T range are in general agreement (within the errors) with the indications from the late T dwarfs alone from Pinfield et al. (2008) and Burningham et al. (2010a), such that $\alpha < 0$. Indeed both our L-T transition sample and the late T dwarf samples are suggestive of $-1 < \alpha < 0$. A better constraint on the binary fraction, as well as a larger sample size however, is required before we can place robust constraints on the form of the brown dwarf birth rate, other than to suggest that a halo form of the birth rate is extremely unlikely.

ACKNOWLEDGMENTS

ADJ is supported by a FONDECYT postdoctorado fellowship under project number 3100098. ADJ is also partially supported by the Joint Committee ESO-Government of Chile. JJ is also supported by a FONDECYT postoctorado fellowship (project number 3110004). ADJ, JJ and MTR would also like to acknowledge the support of the grant from CONICYT and the partial support from Center for Astrophysics FONDAP and Proyecto Basal PB06 (CATA). ADJ and JJ are also partially supported by the Joint Committee ESO-Government of Chile. JG is supported by RoPACS, a Marie Curie Initial Training Network funded by the European Commission's Seventh Framework Programme. SC is supported by a Marie Curie Intra-European Fellowship within the 7th European Community Framework Programme. This research has benefited from the SpeX Prism Spectral Libraries, maintained by Adam Burgasser at http://pono.ucsd.edu/∼adam/browndwarfs/spexprism.

REFERENCES

Allard F., Hauschildt P.H., Alexander D.R., Starrfield S., 1997, ARA&A, 35. 137
Allen P.R., Koerner D.W., Reid I.N., Trilling D.E., 1995, ApJ, 625, 385
Baraffe I., Chabrier G., Barman T. S., Allard F., Hauschildt P. H., 2003, A&A, 402, 701
Baraffe I., 2010, HiA, 15, 755
Bate M.R., Bonnell I.A., Bromm V., 2002, MNRAS, 322, 65
Bate M.R., Bonnell I.A., Bromm V., 2003, MNRAS, 339, 577
Boffin H.M.J., et al., 1998, MNRAS, 300, 1189
Burgasser A. J., Kirkpatrick J.D., Reid I.N., Brown M.E., Miskey C.L., Gizis J.E., 2003, ApJ, 586, 512
Burgasser A.J., et al., 2003, ApJ, 592, 1186
Buragsser A.J., 2004, ApJ, 155, 191

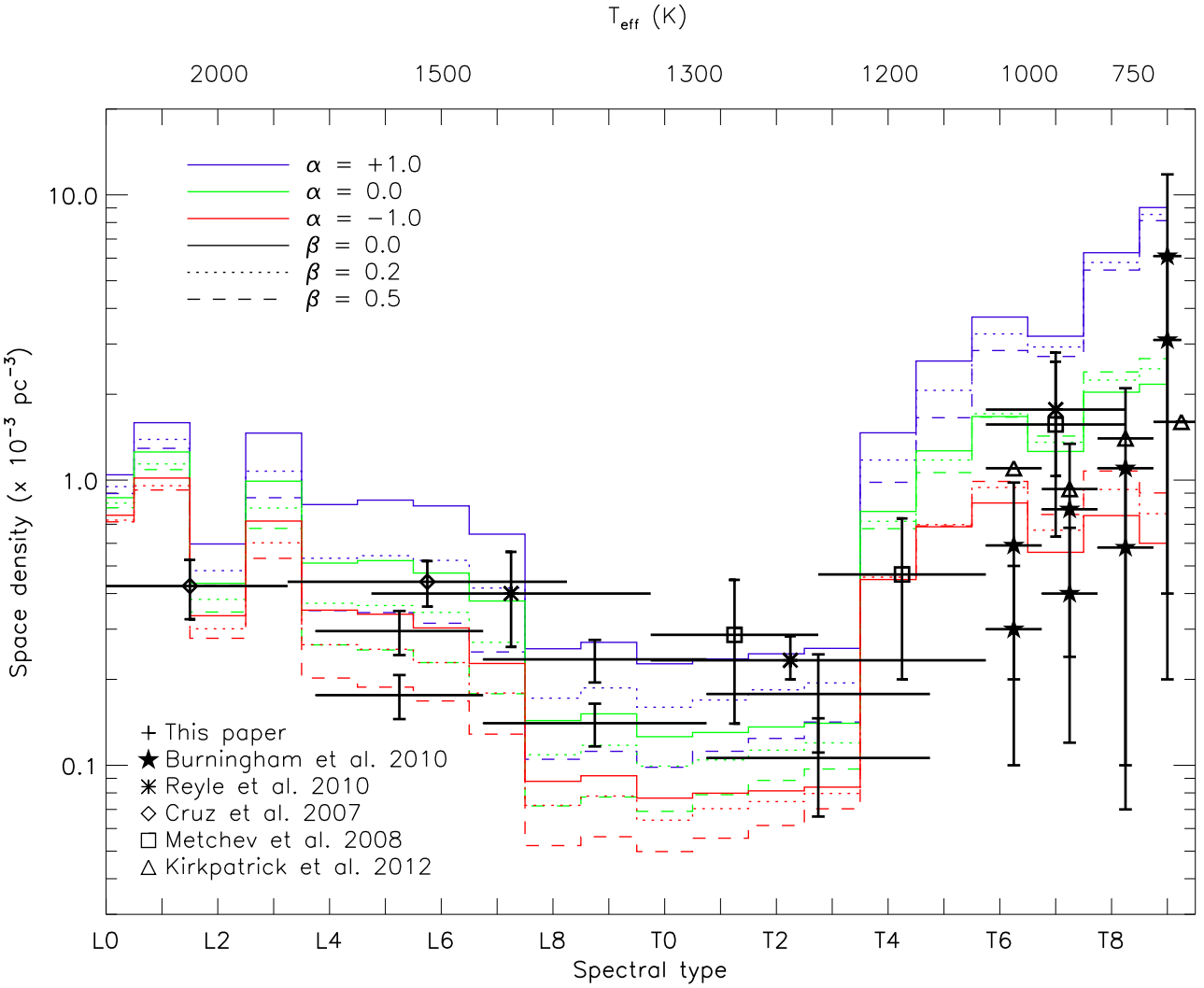

Figure 13. Our sub-sample of mid L-mid T dwarfs are overplotted with simulations from Deacon & Hambly (2006) with $\alpha = +1.0$, 0.0, -1.0 and $\beta = 0.0$, 0.2, 0.5 (where $\psi(M) \propto M^{-\alpha}$). Upper most points of the bins represent a binary fraction of 5% and the lower points are for a binary fraction of 45%.

Burgasser A.J., McElwain M.W., Kirkpatrick J.D., Cruz K.L., Tinney C.G., Reid I.N., 2004, AJ, 127, 2856

Burgasser A.J., Geballe T.R., Leggett S.K., Kirkpatrick J.D., Golimowski D.A., 2006, ApJ, 637, 1067

Burgasser A.J., McElwain M.W., 2006, AJ, 131, 1007

Burgasser A.J., 2007, ApJ, 659, 655

Burgasser A.J., Looper D.L., Kirkpatrick J.D., Liu M.C., 2007, 658, 557

Burgasser A.J., Liu M.C., Ireland M.J, Cruz K.L., Dupuy T.J., 2008, ApJ, 681, 579

Burgasser A.J., Cruz K.L., Cushing M., Gelino C.R., Looper D.L., Faherty J.K., Kirkpatrick J.D., Reid I.N., 2010, ApJ, 710, 1142

Burningham B., et al., 2009, MNRAS, 395, 1237

Burningham B, et al., 2010a, MNRAS, 406, 1885

Burningham B, et al., 2010b, MNRAS, 404, 1952

Cignoni M., Degl'Innocenti S., Prada Moroni P.G., Shore S.N., 2006, A&A, 459, 783

Chabrier G., 2002, ApJ, 567, 304

Chabrier G., 2001, ApJ, 554, 1274

Chiu K., Fan X., Leggett S.K., Golimowski D.A., Zheng W., Geballe T.R., Schneider D.P., Brinkmann J., 2006, AJ, 131, 2722

Caballero J. A., López-Santiago J., de Castro E., Cornide M., 2009, AJ, 137, 5012

Clarke J.R.A., et al., 2010, MNRAS, 402, 575

Chauvin G., Lagrange A.M., Dumas C., Zuckerman B., Mouillet D., Song I., Beuzit J.L., Lowrance P., 2004, A&A, 425,29

Chiu K., Fan X., Leggett S.K., Golimowski D.A., Zheng W., Geballe T.R., Schneider D.P., Brinkmann J., 2006, AJ, 131, 2722

Cruz K.L., Burgasser A.J., Reid I.N., Liebert J., ApJ, 604, 61

Cruz K.L., et al., 2007, AJ, 133, 439

Cushing M.C., et al., 2011, ApJ, 743, 50

Day-Jones A.C., et al., 2011, MNRAS, 410, 705

Deacon N.R., Hambly N.C., 2006, MNRAS, 371, 1722

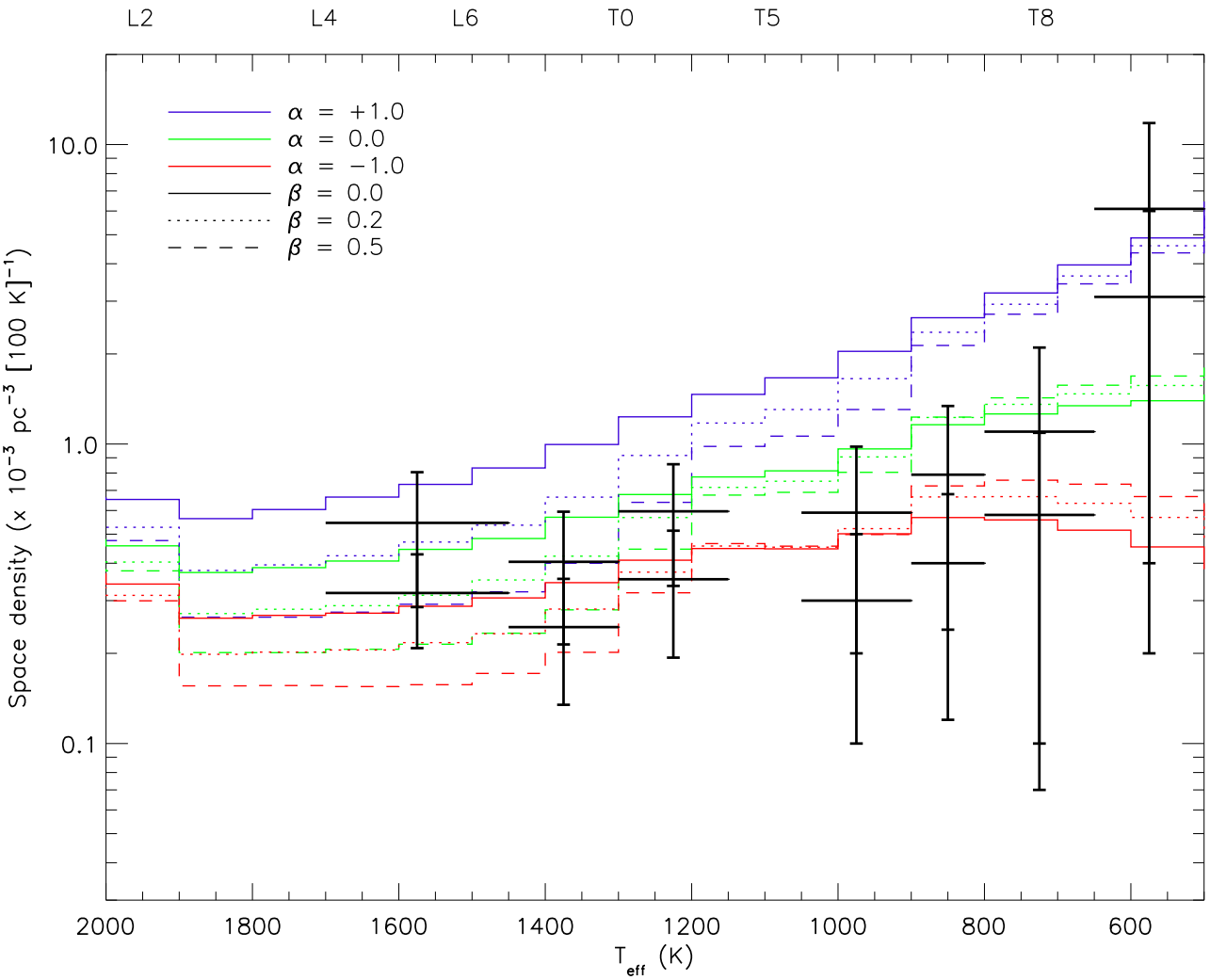

Figure 14. Our sub-sample of mid L-mid T dwarfs are overplotted with simulations from Deacon & Hambly (2006) with $\alpha = +1.0$, 0.0, -1.0 and $\beta = 0.0$, 0.2, 0.5 (where $\psi(M) \propto M^{-\alpha}$). With bins of 1700-1450K, 1450-1300K and 1300-1150K, and 500-1100K for late type T dwarfs as taken from Burningham et al. (2010a). Upper most points of the bins represent a binary fraction of 5% and the lower points are for a binary fraction of 45%.

Deacon N.R., Nelemans G., Hambly N.C., A&A,486, 283

Delgado-Donate E.J., Clarke C.J., Bate M. R., 2003, MNRAS, 342, 926

Emerson J., & Sutherland W., 2003, Proc of SPIE, 4836, 35

Fukugita M., Ichikawa T., Gunn J.E., Doi M., Shimasaku K., Schneider, D. P., AJ, 111, 1748

Gálvez-Ortiz M.C., et al, 2010, MNRAS, 409, 552

Geballe T.R., Knapp G.R., Leggett S.K., Fan X., Golimowski D.A., Anderson S., Brinkmann J., Csabai I., et al., 2002, ApJ, 564, 466

Geißler K., Metchev S., Kirkpatrick J. D., Berriman G. B., Looper D., 2011, ApJ, 732, 56

Hawley S.L., et al., 2002, AJ, 123, 3409

Hewett P.C., Warren S.J., Leggett S.K., Hodgkin S.T., 2006, MNRAS, 367, 454

Kirkpatrick J.D., Reid I.N., Liebert J., Gizis J.E., Burgasser A.J., Monet D.G., Dahn C.C., Nelson B., Williams R.J., 2000, AJ, 120, 447

Kirkpatrick J.D., et al., 2010, ApJS, 190, 100

Kirkpatrick J.D., Cushing M.C., Gelino C.R., Griffith R.L., Skrutskie M.F., Marsh K.A., Wright E.L., Mainzer A., et al., 2011, ApJS, 197, 19

Kirkpatrick J.D., et al., 2012, ApJ, 753, 156.

Kirkpatrick J.D., et al., 1999, ApJ, 519, 802

Knapp G.R., et al., 2004, ApJ, 127, 3553

Lafreniére D., Jayawardhana R., van Kerkwijk M.H., 2008, ApJ, 689, 153

Lawrence A., et al., 2007, MNRAS, 379, 1599

Lodieu N., Caux E., Monin J.L., Klotz A., 2002, A&A, 383,15

Lodieu N., Hambly N.C., Jameson R.F., Hodgkin S.T., Carraro G., Kendall T.R., 2007, MNRAS, 374, 372

Lodieu N., Hambly N.C., Jameson R.F., Hodgkin S.T., 2008, MNRAS, 383, 1385

Lodieu N., Zapatero Osorio M.R., Martin E.L., Solano E.,

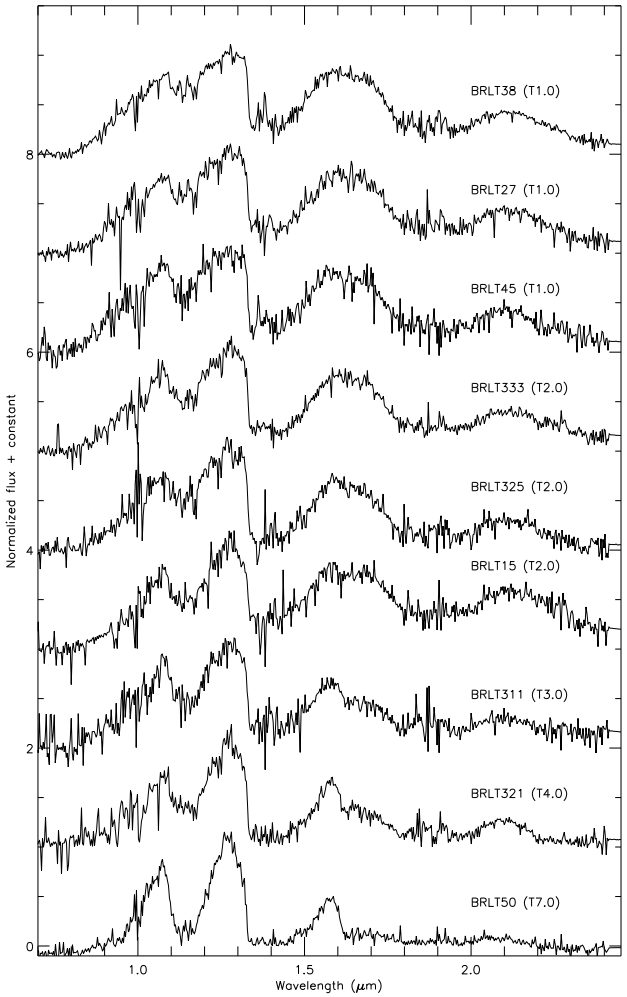

Figure 9. X-shooter spectra of L and T dwarfs from birth rate sample, in ascending spectral type.

Aberasturi M., 2010, ApJ, 708,107
Looper D.L., Kirkpatrick J.D., Burgasser A.J., 2007, AJ, 134, 1162
Luhman K.L., et al., 2009, ApJ, 666, 1219
Luhman K.L., 2007, ApJS, 173,104
Marocco F., et al., 2010, A&A, 524, 38
Maxted P.F.L., Jeffries R.D., 2005, MNRAS, 362, 45
Metchev S.A., Kirkpatrick J.D. Berriman G.B, Looper D., 2008, ApJ, 676, 1281
Miller G.E., Scalo J.M., 1979, ApJS, 41, 513
Murray D.N., et al., 2011, MNRAS, 414, 575
Oliveira J.M., Jeffries R.D., van Loon J.Th., 2009, MNRAS, 329, 1034
Padoan P., Nordlund A., 2002, ApJ, 576, 870
Padoan P., Nordlund A., 2004, ApJ, 617, 559
Pinfield D.J., et al., 2008, MNRAS, 390, 304
Quanz S.P., Goldman B., Henning T., Brandner W., Burrows A., Hofstetter L.W., 2010, ApJ, 708,770
Reid I.N., Gizis J., 1997, AJ, 113, 2246
Reid I.N., Lewitus E., Burgasser A.J., Cruz K.L., 2006, ApJ, 639, 1114
Reid I.N., Gizis J., & Hawley S., 200, AJ, 124,2721
Reid I.N., et al., 1999, ApJ, 521, 613
Reipurth B., Clarke C.J., 2001, AJ, 122, 432
Reylé, C., Delorme P., Willott C.J., Albert L., Delfosse X., Forveille T., Artigau E., Malo L.,et al., 2010, A&A, 522, 112
Rocha-Pinto H.J., Scalo J., Maciel W.J., Flynn C., 2000, A&A, 358, 869
Salpeter E.E., 1955, VA, 1, 283
Schmidt S.J., West A.A., Hawley S.L., Pineda J.S., 2010, AJ, 139, 1808
Scholz R.D., 2010, A&A, 510, 8
Stephens D. C., et al., 2009, ApJ, 702, 154
Skrutskie M.F., et al., 2006, AJ, 131, 1163
Sterzik M.F., Durisen R.H., 2003, A&A, 400, 1031
Warren S., Dye S., Hambly N., 2006, Msngr, 123,67
Whitworth A.P., Goodwin S.P., 2005, AN, 326, 899
Whitworth A.P., Zinnecker H., 2004, A&A, 427, 299
Whitworth A.P., Stamatellos D., 2006, A&A, 458, 817
Wright E.L., Eisenhardt P.R.M., Mainzer A.K., Ressler M. E., Cutri R.M., Jarrett T., Kirkpatrick J.D., Padgett D., et al., 2010, AJ, 140, 1868
Wyse R.F.G., 2008, ASPC, 399, 445
Zhang Z.H., et al., 2010, MNRAS, 404, 1817

This paper has been typeset from a TEX/ LATEX file prepared by the author.